nature geoscience

SUPPLEMENTARY INFORMATION

https://doi.org/10.1038/s41561-019-0353-3

In the format provided by the authors and unedited.

Higher frequency of Central Pacific El Niño events in recent decades relative to past centuries

Mandy B. Freund[1,2,3*], Benjamin J. Henley[1,2,4,5], David J. Karoly[1,2,6], Helen V. McGregor[7], Nerilie J. Abram[8,9] and Dietmar Dommenget[5,10]

[1]School of Earth Sciences, University of Melbourne, Parkville, Victoria, Australia. [2]ARC Centre of Excellence for Climate System Science, University of Melbourne, Parkville, Victoria, Australia. [3]Climate and Energy College, University of Melbourne, Parkville, Victoria, Australia. [4]ARC Centre of Excellence for Climate Extremes, University of Melbourne, Parkville, Victoria, Australia. [5]School of Earth, Atmosphere and Environment, Monash University, Clayton, Victoria, Australia. [6]NESP Earth Systems and Climate Change Hub, CSIRO, Aspendale, Victoria, Australia. [7]School of Earth, Atmospheric and Life Sciences, University of Wollongong, Wollongong, New South Wales, Australia. [8]Research School of Earth Sciences, Australian National University, Canberra, Australian Capital Territory, Australia. [9]ARC Centre of Excellence for Climate Extremes, Australian National University, Canberra, Australian Capital Territory, Australia. [10]ARC Centre of Excellence for Climate Extremes, Monash University, Clayton, Victoria, Australia. *e-mail: freundm@unimelb.edu.au

Contents

1 Methodological Framework

A step-by-step schematic of our approach is illustrated in Figure S1. Based on a seasonally-resolved network of coral records and in conjunction with the seasonal instrumental target indices, we reconstruct El Niño variability back in time. We train and apply a decision tree which classifies Eastern Pacific (EP) and Central Pacific (CP) El Niño events based on two reconstructed time series. This allows us to draw conclusions about past behaviour of El Niño in terms of event types and frequencies. Individual intermediate steps are listed below and details are given in the method descriptions that follow. Methodological choices and data limitations are also assessed for their impacts on our conclusions, using a number of sensitivity experiments, as documented here.

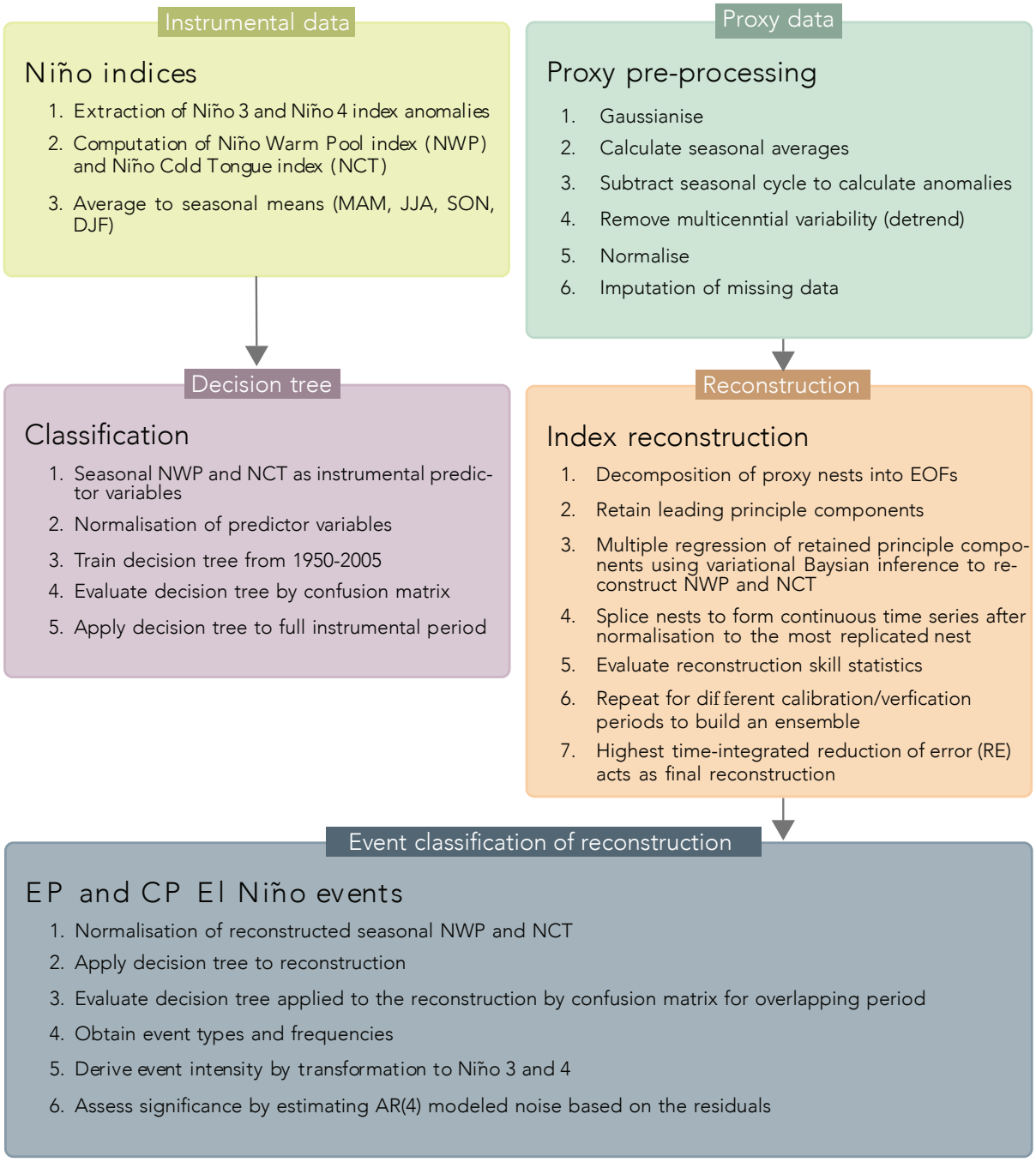

Figure S1. Schematic overview of the study. From the input datasets (proxy data & instrumental data), the reconstruction method and application of the decision tree to the event classification, that is been done separately for the instrumental and reconstructed records.

2 El Niño diversity in the instrumental record

2.1 Instrumental ENSO Indices

ENSO activity is typically monitored by the leading modes of SST variability of the tropical Pacific (e.g. "EPI" [1], "CPI" [2]) and regional averages over Niño regions (e.g. Niño3.4 [3], "TNI" [4], "EMI" [5]). Limited by orthogonality constraints in time and space, seasonal and spatial representation, the Niño Warm Pool index (NWP) and Niño Cold Tongue index (NCT) [6] describe sufficiently the time evolution and characteristic pattern for both ENSO types on a seasonal timescale. We compute NWP and NCT from the monthly Hadley Centre Sea Ice and Sea Surface Temperature (HadISST) dataset [3] from 1870-2015 (http://www.metoffice.gov.uk/hadobs/hadisst/) as:

$$\begin{aligned} N_{CT} &= N_3 - \alpha N_4 \\ N_{WP} &= N_4 - \alpha N_3, \end{aligned} \qquad \alpha = \begin{cases} 2/5 & \text{for } N_3 N_4 > 0 \\ 0 & \text{otherwise} \end{cases} \tag{1}$$

where N_3 and N_4 are the mean SST in the Niño-3 and Niño-4 regions respectively.

Table S1. Comparison of ENSO indices Pearson correlation coefficients of the Niño Warm Pool index (NWP) and Niño Cold tongue index (NCT) with different ENSO indices during the instrumental period (1950-2014).

	NCT	NWP
Nino1.2	0.9	0.1
Nino3	0.9	0.4
Nino4	0.6	0.8
TNI	0.4	-0.7
MEI	0.8	0.5
EMI	-0.0	0.8

The number of observations contributing to the observed SST dataset HadISST is shown in Fig. S2. The number of observed grid boxes in the Niño 3 and 4 regions reaches at least 50% of the grid boxes in the regions after approximately 1920. The seasonal signatures in both regions are considered therefore to be sufficiently observed to provide a reliable source of SST variability after that time, noting that in general the observational coverage of the Niño 3 region is better than in the Niño 4 region. After 1920, the number of well-observed grid boxes in the Niño regions stays relatively constant and improves, apart from a scarcity of observations during the Second World War. This is in line with analysis done by refs. [7;8].

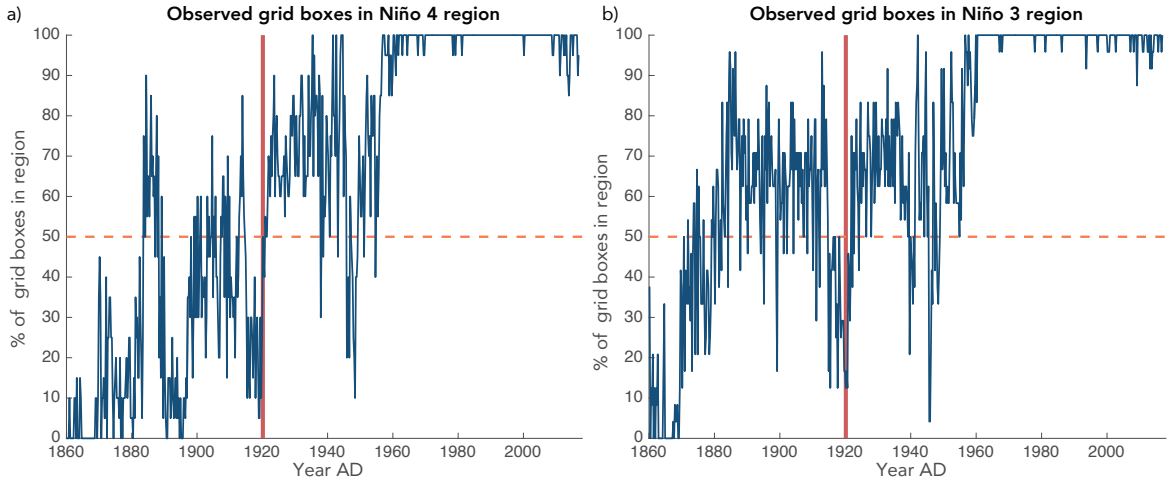

Figure S2. Observations in the Niño 3 and 4 region Coverage of observations given as percentages of 5 °grid boxes in the Niño 4 region (**a**) and Niño 3 regions (**b**). Observations are estimated for seasonal averages for MAM, JJA, SON and DJF based on HadCRUT4 ref. [9]. Red lines highlights 1920 with 50% grid boxes and above.

2.1.1 Instrumental dataset

Historical SST datasets in data sparse regions can vary extensively due to different underlying data and methodologies[10]. We examine the sensitivity of our reconstruction and classification method to the target indices based on HadISST (as used in the main paper) and ERSST[11] instrumental datasets. During the instrumental period, the ERSST[11] and HadISST-derived reconstructed indices and classification results show little difference. A number of El Niño events in the ERSST reconstruction show slightly larger amplitudes than the HadISST reconstruction. The ERSST reconstructions show only small differences in terms of variance and event amplitude (Figure S3 c-g). The application of the classification tree using ERSST identifies 92% of the EP events that are identified by the HadISST-based reconstruction during the entire reconstruction period. This number is reduced to 64% for the CP El Niño events prior to 1900. Nevertheless, the direct comparison of the number of EP and CP events over time shows a similar evolution. The low number of EP and CP El Niño events during the 1670-1690 period in the HadISST-based reconstruction is also produced in the ERSST reconstruction. Marked differences are only observable for the absolute amplitudes (Figure S3e,f). However, the EP El Niño events of 1997 and 1982 exceed all of the inferred reconstructed event amplitudes. Therefore our key conclusions remain unchanged when considering different instrumental datasets.

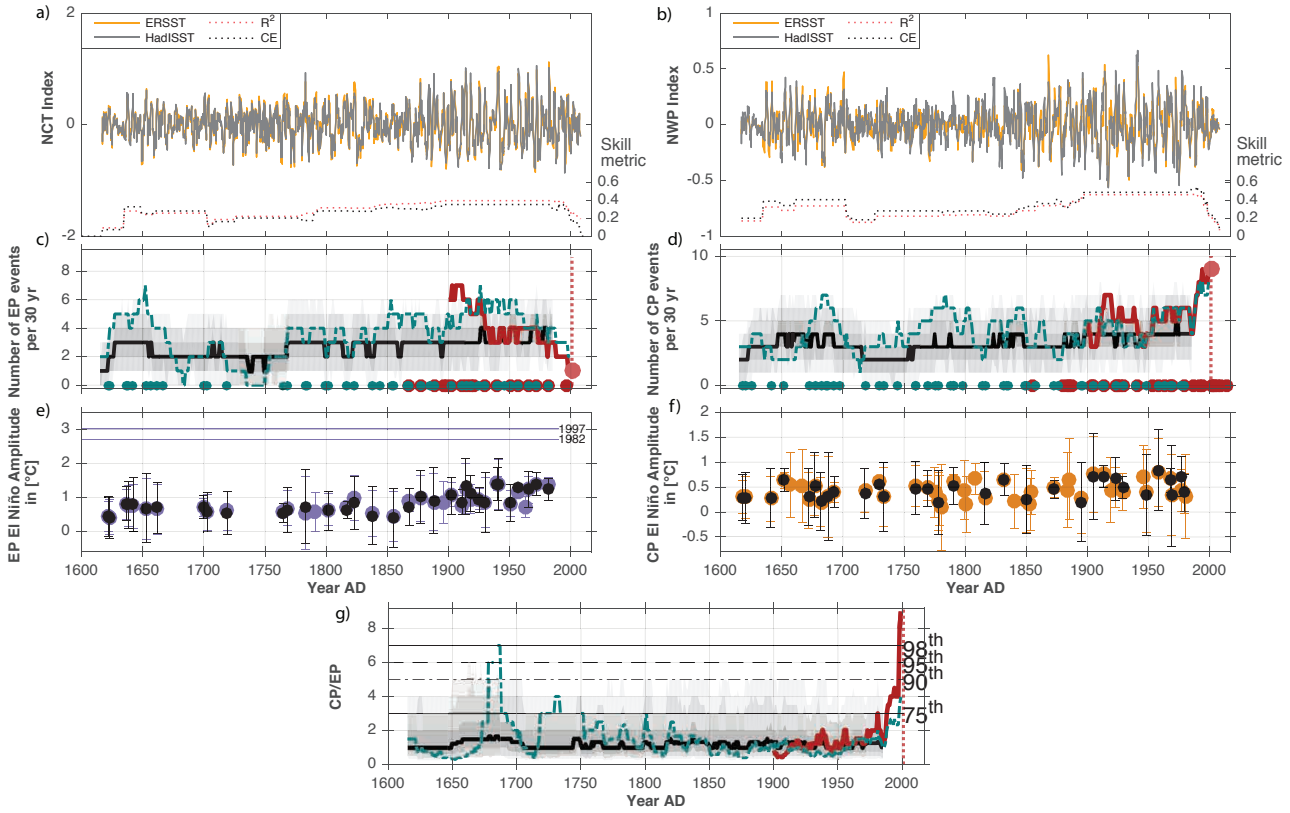

Figure S3. Sensitivity of reconstruction to instrumental target Comparison between NCT (**a**) and NWP (**b**) index reconstructions base on HadISST and ERSST, including skill metrics on secondary axis ($\delta^{18}O$ records only). Number of CP El Niño (ERSST) (**c**), EP El Niño events (ERSST) (**d**) and ratio of CP to EP events (ERSST) (**g**) in sliding 30-yr windows; instrumental ERSST (red), most-replicated reconstruction (teal), bootstrapped median (black) and uncertainty range in grey shadings (75^{th}, 90^{th}, 95^{th} percentiles) shown. Event amplitudes for EP (**e**) and CP El Niño events (**f**) are compared based on all records HadISST (colored) and ERSST (black). Error bars indicate 95% confidence interval from bootstrapping.

2.2 Conditions during EP and CP El Niño events

The two types of El Niño differ substantially in terms of their dynamics and impacts (Supplementary Figure S7 & S8). The seasonal evolution of SST anomalies during eastern Pacific El Niño events shows warm SST

anomalies near the South American coast propagating westward along the equator [12] (Supplementary Figure S5). Sea surface salinity (SSS) observations also show a contrasting pattern in the equatorial Pacific of the warm pool and along the mean SPCZ position. Similar to findings by ref. [13], both EP and CP events can result in a decrease of SSS (freshening) near the dateline and an increase of SSS in the SPCZ region, but EP events are associated with a up to 2-3 times stronger SSS increase in the SPCZ region and a larger eastward displacements of the eastern edge of the low- salinity warm pool waters in the equatorial band compared to CP El Niño events. The seasonal impacts of EP and CP El Niño events are shown by the precipitation and temperature anomaly patterns in Supplementary Figure S7 & S8. The Niño warm pool (NWP) and Niño cold tongue (NCT) index are related to the spatial structures derived from the composite analysis. Both indices represent the sea surface anomalies patterns during EP and CP events best when correlated with SSTA (Supplementary Figure S4a,b). Similarly to the composite pattern are the two indices related to changes in sea surface salinity (SSS) (Supplementary Figure S4c,d) and precipitation (Supplementary Figure S4e,f) which are interrelated vice versa.

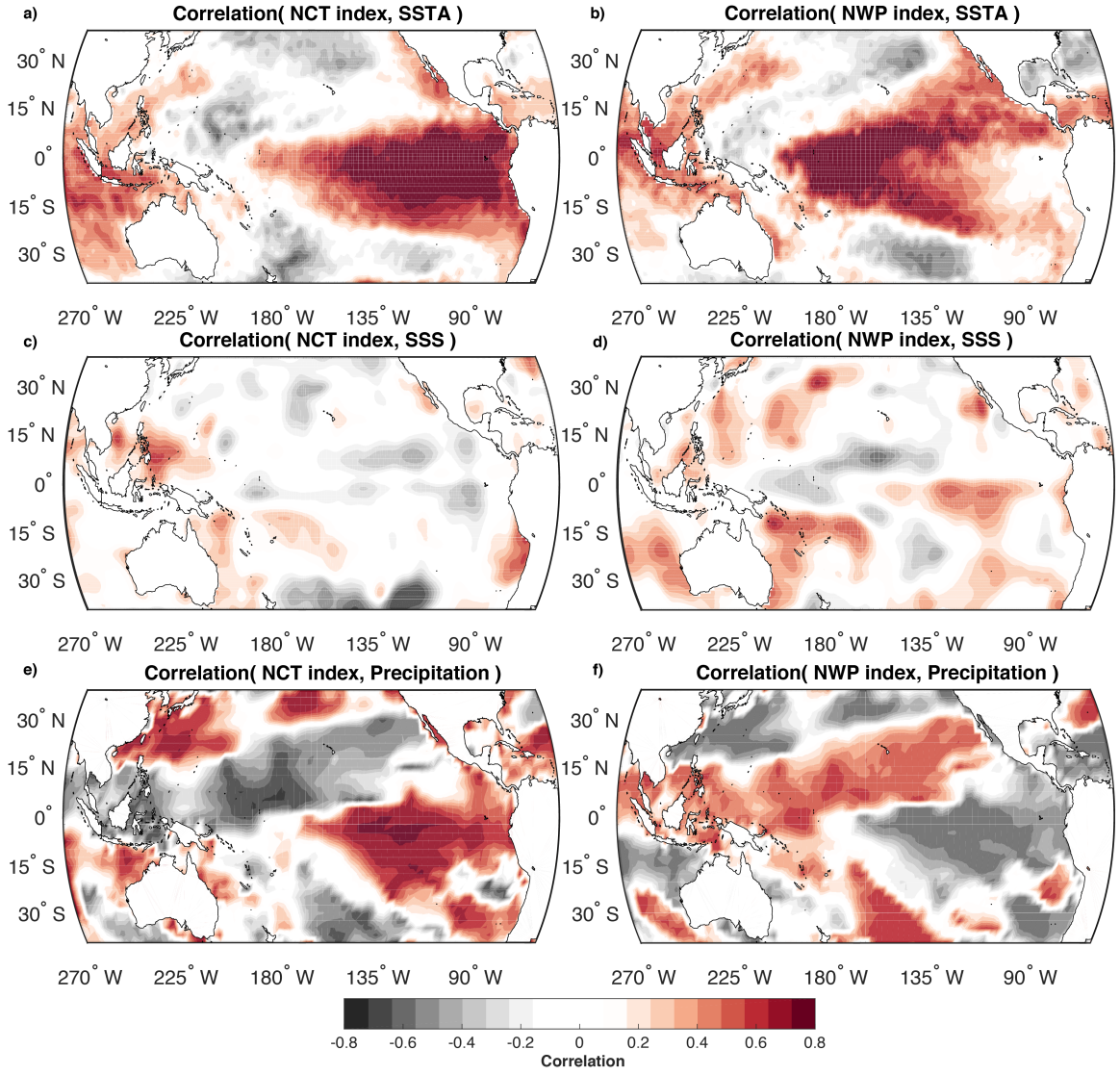

Figure S4. Spatial correlations of NCT and NWP. Spatial correlations of NCT and NWP with sea surface temperature anomalies **a,b**, sea surface salinity **c,d** and precipitation anomalies **e,f**, respectively. Each monthly dataset was detrended to remove any long-term trends prior to correlation analysis. The sea surface temperature anomalies (SSTA) are derived from the HadISST dataset [3], the sea surface salinity dataset (SSS) is derived from the SSS Had EN4.2.0 dataset [14], which uses objective analysis formed from profile data and precipitation anomalies are derived from GPCP2.3 [15], relative to AD $1950-2015$ means.

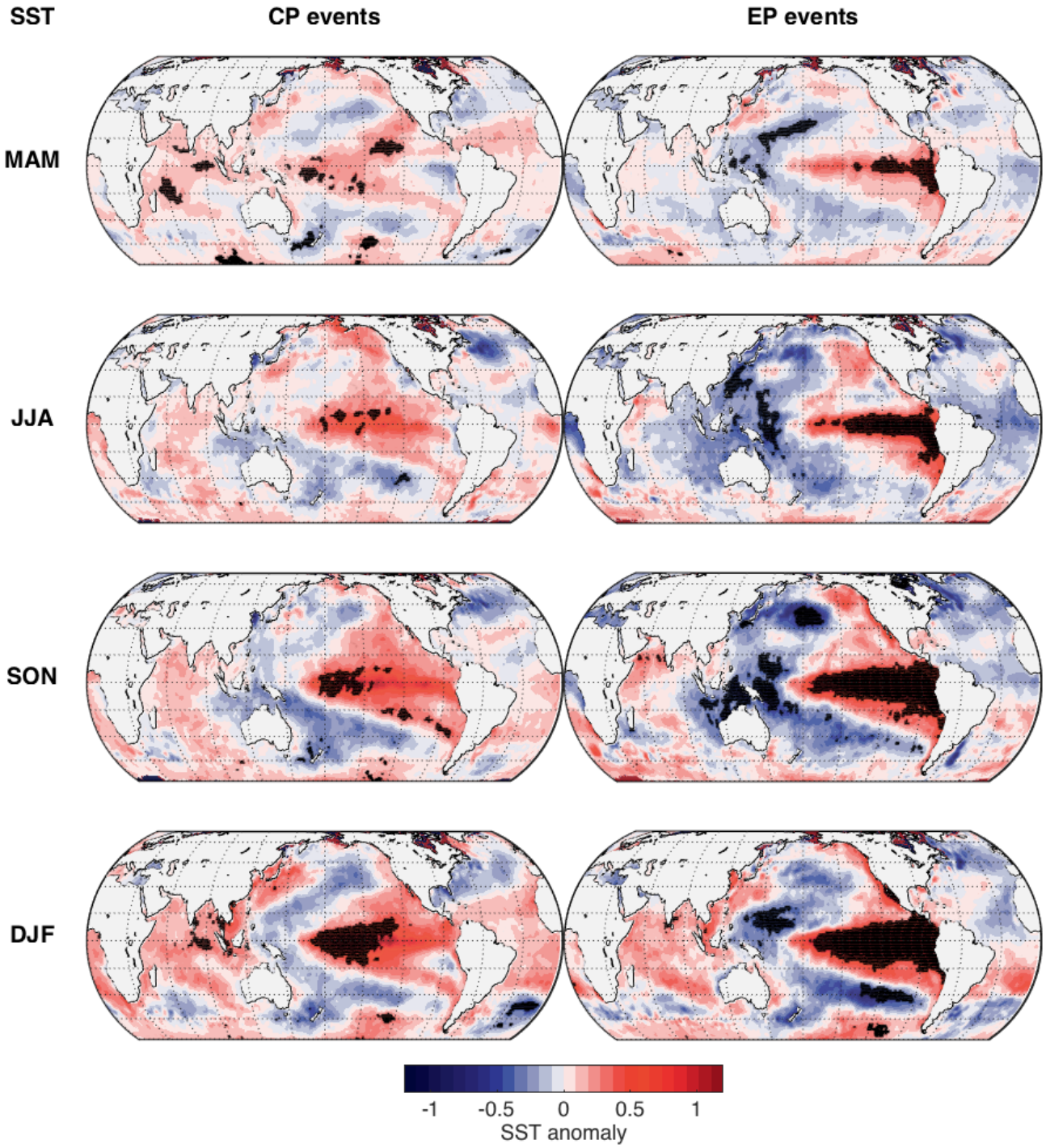

Figure S5. Seasonal composites of sea surface temperature anomalies in EP and CP El Niño events. Composites of seasonal SSTA for CP El Niño (1963, 1968, 1977, 1979, 1987, 1991, 1994, 2002, 2004, 2009) and EP El Niño events (1951, 1957, 1965, 1972, 1976, 1982, 1986, 1997). SSTA derived from HadISST relative to AD 1950 – 2015 means. Stippling indicates statistically significant ($p < 0.05$) anomalies.

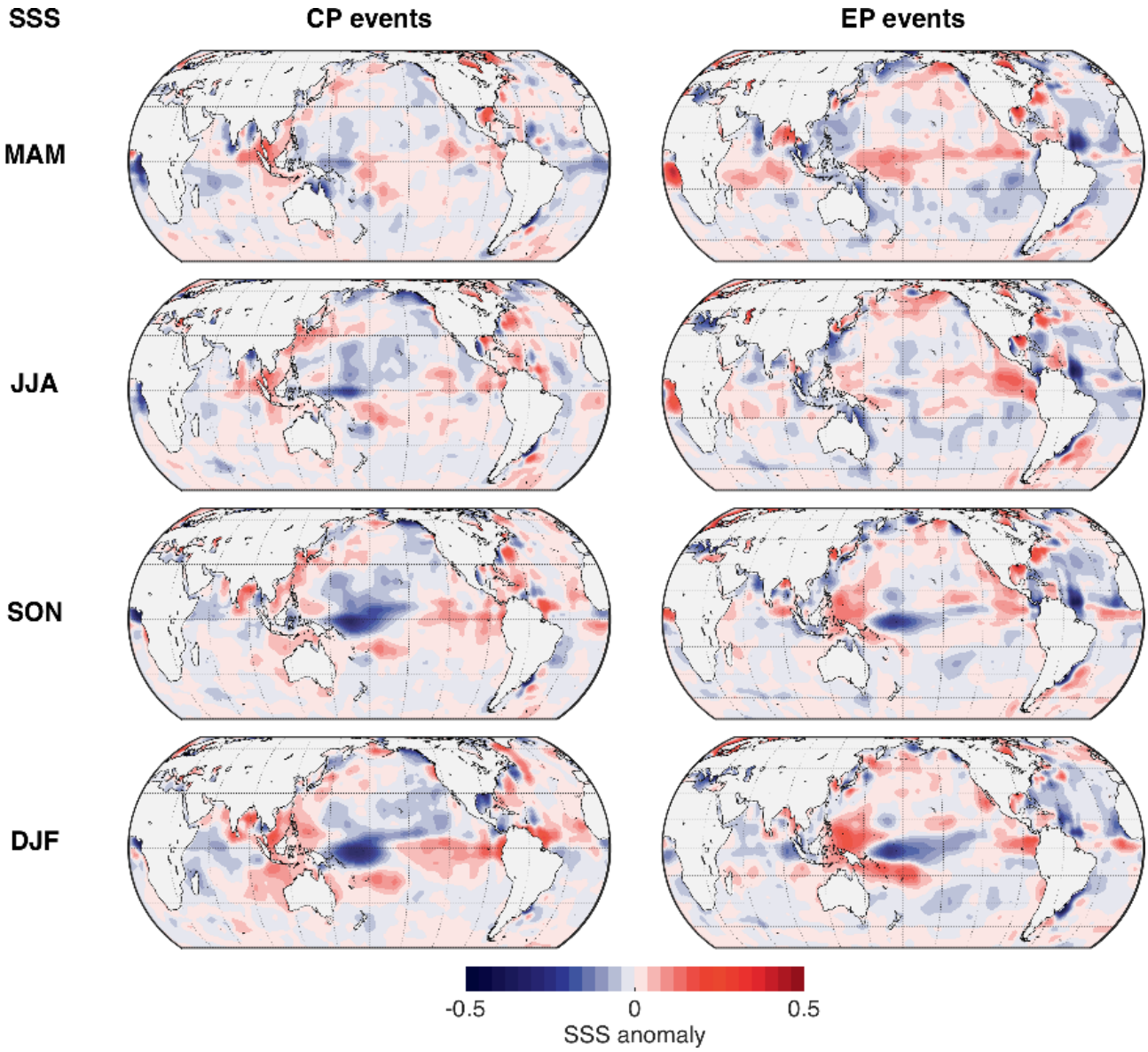

Figure S6. Seasonal composites of salinity anomalies in EP and CP El Niño events. Composites of seasonal SSSA for CP El Niño (1963, 1968, 1977, 1979, 1987, 1991, 1994, 2002, 2004, 2009) and EP El Niño events (1951, 1957, 1965, 1972, 1976, 1982, 1986, 1997). SSSA derived from Had EN4.2.0 dataset [14] relative to AD 1950 – 2015 means.

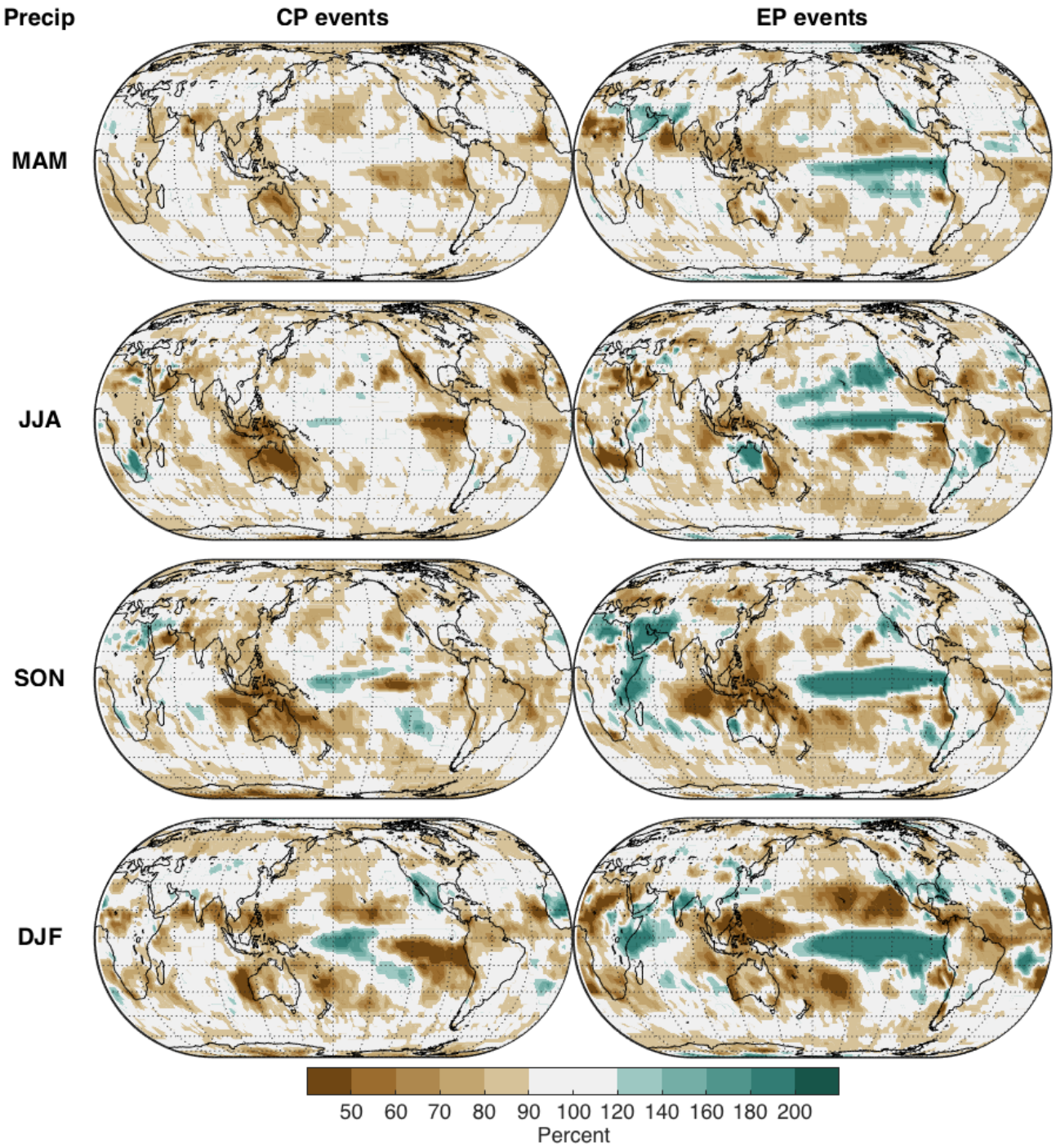

Figure S7. Seasonal composites of precipitation in EP and CP El Niño events. Composites of seasonal precipitation for CP El Niño (1979, 1987, 1991, 1994, 2002, 2004, 2009) and EP El Niño events (1982, 1986, 1997) as a percent of the mean. Precipitation from GPCP2.3 [15], relative to AD 1979 – 2015 means.

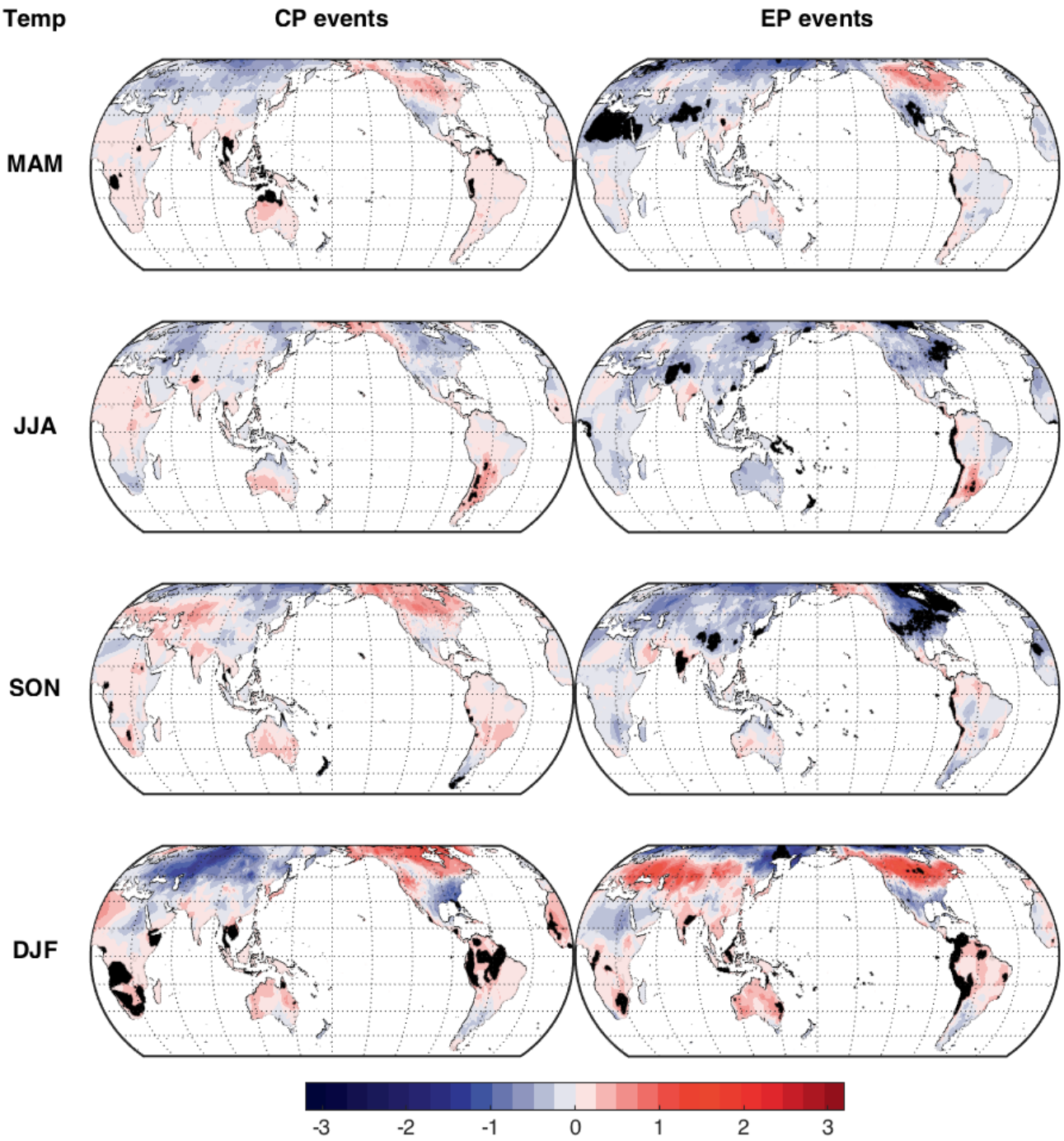

Figure S8. Seasonal composites of surface temperature in EP and CP El Niño events. Composites of seasonal temperature for CP El Niño (1963, 1968, 1977, 1979, 1987, 1991, 1994, 2002, 2004, 2009) and EP El Niño events (1951, 1957, 1965, 1972, 1976, 1982, 1986, 1997). Temperature anomalies are derived from CRUTS3.2 relative to AD $1950-2015$ means. Stippling indicates statistically significant ($p < 0.05$) anomalies.

2.3 Event classification during the instrumental period

The decision tree classifies El Niño events based on the seasonal evolution of the Niño indices. The tree is trained on the instrumental period using the EP and CP events as identified by ref. [16], but excluding weak events. The EP years are: 1951/52, 1957/58, 1965/66, 1972/73, 1976/77, 1982/83, 1986/87, 1997/98 and the CP years are: 1963/64, 1968/69, 1977/78, 1979/80, 1987/88, 1991/92, 1994/95, 2002/03, 2004/05. A comparison of the events identified by previous studies is shown in Fig. S9 b) [17–21].

There is generally clear agreement between previous studies about the EP/CP classification of instrumental period El Niño events despite differing methodological approaches and subjective thresholds (Supplementary Fig. S9 b). For example, the EP events in 1982/83 and 1997/98, and CP events in 2002/03 & 2004/05 are consistently identified across the studies.

We have excluded the weak CP El Niño years 1990/91, 1992/93 and 1993/94 from our analysis. The majority of previous studies do not identify these years as CP events [22]. Some studies suggest that these years were of CP El Niño character [1;2;5;6], or reported as consecutive CP events.

Considering the seasonal anomalies of the Ocean Niño Index (ONI; 3 month running mean of SST anomalies averaged in the Niño 3.4 region), often used to monitor both types of El Niño in the Pacific, these weak CP years do not show unusual anomalies (Supplementary Fig. S9 a). Our classification approach is therefore trained on a conservative estimate of EP and CP years.

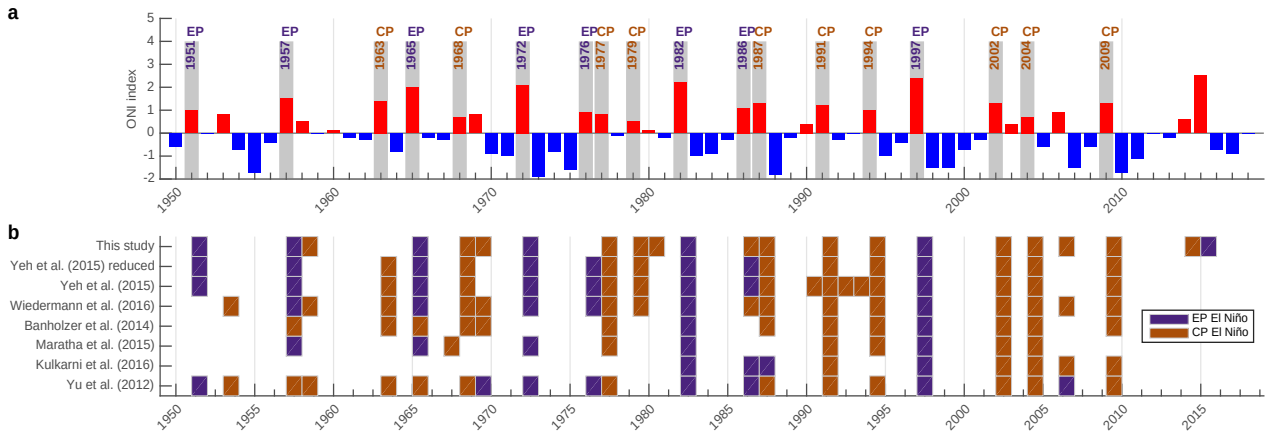

Figure S9. EP and CP El Niño classification during the instrumental period. **a,** Oceanic Niño Index (ONI) based on 3 month running mean of ERSST.v5 SST anomalies in the Niño 3.4 region. The ONI is shown as positive (red) and negative (blue) deviations from a centered 30-year base period for SON. EP and CP event years are highlighted according to this study following [23]. **b,** EP and CP El Niño years used in this study comapred with different classification approaches according to ref [23], ref [17], ref [18], ref [19], ref [20] and ref [21].

3 Proxy network

3.1 Coral records of $\delta^{18}O$ and Sr/Ca

A network of 27 high-resolution coral-derived records is compiled, including 23 stable oxygen isotope ($\delta^{18}O$) and 4 strontium-calcium (Sr/Ca) ratio coral records from sites in the tropical Pacific and eastern Indian Oceans (Supplementary Table S2). The Sr/Ca ratio records of skeletal aragonite are predominately a function of sea surface temperature[24], while stable oxygen isotope $\delta^{18}O$ records can be related to multiple factors of the coupled ocean-atmosphere system (primarily SST and $\delta^{18}O$ seawater).

3.1.1 $\delta^{18}O$ in coral records

The isotopic signature of $\delta^{18}O$ in carbonates of coral records ($\delta^{18}O_C$) is used to infer the seawater temperature and $^{18}O_{SW}$ conditions in the past. The ratio of oxygen isotopes in marine carbonates (e.g. aragonite) preserved in the coral banding is determined by the source isotopic composition of surrounding seawater $^{18}O_{SW}$ and the equilibrium isotopic fractionation, inversely related to temperature between the seawater and carbonate[25]. The oxygen isotopes are fractionated through the annual cycle and the $\delta^{18}O_{SW}$ is affected by advection of water masses with different isotope signatures, and precipitation-evaporation (P-E) changes. P-E changes also affect SSS so $\delta^{18}O$ is often used as a SST, SSS or SST-SSS proxy, depending on the location. The exact relationship between salinity and $^{18}O_{SW}$ is complex and can depend on local conditions[26]. In general, if sea surface salinity is relatively constant, $\delta^{18}O_C$ in corals are mainly determined by SST variability and vice versa. At the same time, highly variable SSS and SST variations can make the interpretation of $\delta^{18}O_C$ more complex[26].
All of the 27 considered coral records are reported to be linked to ENSO variability (Table S3, "Reported interannual signal"). Spatial correlation maps for each site confirms high correlations with basin-wide variability pattern for SST and SSS (Fig. S12 and S14). Most of the site maps show higher correlations with the basin-wide SST pattern than SSS pattern. The analysis of the coral records shows that most interannual variability is related local and basin-wide variability of sea surface temperatures, but also show co-variations with salinity and precipitation in particular for $\delta^{18}O$ records (Table S3).
Twenty-two of the 23 coral $\delta^{18}O$ records are reported to reflect SST variability (Table S3). Four records (Savusavu Bay, Secas Island, Rarotonga and Tarawa Atoll) are also reported to co-vary with SSS, confirmed by our correlation analysis. In addition, our analysis shows that coral $\delta^{18}O$ at the sites Vanuatu, Double Reef and Palau have higher correlations with local salinity than with SST at interannual time scale and are reported as "mixed signals" of SST and SSS in the original publications. The exclusion of these records from our reconstruction does not alter the main findings (Fig.S26). Mixed SST and salinity variability contributed by these records appears to slightly enhance reconstructed NCT variance but does not have a significant influence on the intensity of El Niño events derived from the reconstructed indices considering the range of uncertainty.
The majority of proxy records remain strongly correlated with the local SSTs (Fig. S3), the spatial fields of SST variability (Fig. S12 and S14) and ENSO variability, including precipitation and salinity influences and other oceanic and atmospheric indices. Together, this suggest strong links between each record and ENSO variability (Table S4). The NWP and NCT indices that are the targets of the reconstruction reflect both SST variability and changes in SSS and precipitation shown by Figure S4. Composite maps for SSTA (Fig. S5), SSS (Fig. S6), temperature (Fig. S8) and precipitation (Fig. S7) as well as instrumental studies highlight that the different types of El Niño not only result in different SST pattern but also covary with different SSS[13] and precipitation pattern (e.g ref.[1;27]). Our analysis of raw SST, SSS and coral $\delta^{18}O$ covariability give confidence in the ability of our network to capture ENSO changes.

3.2 Coral network and data pre-processing

The temporal resolution and location of the coral network is given in Table S2 & S4 and Figure S11. The temporal resolution within the coral network differs substantially, from 4 samples/yr up to 12 samples/yr. Two records are unevenly sampled. We subsample the records onto a regular time grid of 4 samples a year using a weighted averaging procedure (Eq. 2). Within a seasonal window (three consecutive months) samples are averaged by a weighting factor of w = 1. A further weighting factor of w = 0.5 is applied to datapoints within +/- 2 months of the seasonal window, to account for uncertainties in chronologies of the coral records (Fig. S10). The 2-month uncertainty range is derived from two tie point estimates of uncertainty of maximum +/- 56 days[28]. From the seasonal resolution records we calculate anomalies relative to the seasonal cycle.

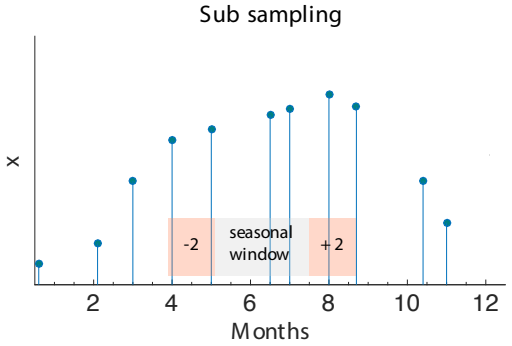

Figure S10. Seasonalising coral records Schematic of pre-processing coral measurements to a common time resolution (seasonal). A weighting procedure is applied to average samples within a seasonal window (three consecutive months). Within the seasonal window, measurements are equally averaged (weighting factor of 1) and during the leading and lagging 2 month period measurements are accounted by a weighting factor of 0.5

$$\bar{x} = \frac{\sum_n^{i=1}(x_i \cdot w_i)}{\sum_n^{i=1} w_i} \qquad (2)$$

After generating seasonal-averages, the records were detrended using a spline filter. Figure S15 shows the raw data, along with seasonalised and detrended pre-processed records.

Table S2. Coral metadata. Details of the seasonally resolved coral network used in this study. Each record is listed by its latitude (Lat), longitude (Lon), the number of measurements per annual year (Res) and if measurements are evenly spaced (Y/N). Absolute correlations between HadISST (1920-1984) at the proxy site (500km radius) and the records are reported from seasonal means (Ann) and for each single season MAM, JJA, SON and DJF, respectively.

Site Name	Country	Proxy	Lat (°N)	Lon (°E)	Res	Evenly spaced	Start Year	End Year	Correlations (SST) Ann	MAM	JJA	SON	DJF	Ref
Palmyra Atoll	USA Territory	$\delta^{18}O$	4.86	197.98	12	Y	1635	1653	-	-	-	-	-	28
Palmyra Atoll	USA Territory	$\delta^{18}O$	4.86	197.98	12	Y	1886	1998	0.75	0.65	0.66	0.80	0.76	28
Savusavu Bay	Fiji	$\delta^{18}O$	-16.14	178.96	8	Y	1617	2001	0.45	0.37	0.52	0.57	0.36	29
New Caledonia	France Territory	Sr/Ca	-22.48	166.46	12	Y	1649	1999	0.55	0.41	0.58	0.63	0.56	30
New Caledonia	France Territory	$\delta^{18}O$	-22.48	166.46	4	Y	1660	1993	0.22	0.32	0.25	0.22	0.10	31
Secas Island	Panama	$\delta^{18}O$	7.00	277.99	10	N	1707	1984	0.24	0.15	0.20	0.19	0.12	32
Rarotonga	Cook Islands	Sr/Ca	-21.04	200.86	8	Y	1726	1997	0.45	0.32	0.30	0.37	0.33	29
Rarotonga	Cook Islands	$\delta^{18}O$	-21.04	200.86	8	Y	1726	1997	0.39	0.36	0.34	0.48	0.35	29
Savusavu Bay	Rep. of Fiji	Sr/Ca	-16.14	178.96	12	Y	1780	1997	0.36	0.23	0.35	0.41	0.34	29
Savusavu Bay	Rep. of Fiji	$\delta^{18}O$	-16.14	178.96	8	Y	1780	1997	0.33	0.34	0.39	0.44	0.44	29
Lombok	Indonesia	$\delta^{18}O$	-8.25	115.50	12	Y	1782	1990	0.15	0.12	0.45	0.33	0.25	33
Bali	Indonesia	$\delta^{18}O$	-8.00	115.00	12	Y	1782	1990	0.15	0.13	0.44	0.31	0.26	33
Double Reef	Guam, USA Territory	$\delta^{18}O$	13.0	145.00	12	Y	1790	2000	0.38	0.49	0.18	0.25	0.45	34
Palau	Rep. of Palau	$\delta^{18}O$	7.29	134.25	12	Y	1793	2008	0.39	0.47	0.18	0.30	0.50	35
Clarion Island	Mexico	$\delta^{18}O$	18.00	245.30	4	Y	1819	1998	0.08	0.10	0.11	0.15	0.19	36
Maiana Atoll	Rep. of Kiribati	$\delta^{18}O$	1.00	173.00	6	Y	1840	1994	0.67	0.53	0.42	0.55	0.62	37
Vanuatu	Rep. of Vanuatu	$\delta^{18}O$	-15.94	166.04	12	Y	1842	2007	0.27	0.21	0.36	0.38	0.34	38
Tonga	Kingdom of Tonga	$\delta^{18}O$	-20.04	185.86	8	Y	1848	2004	0.43	0.29	0.34	0.47	0.32	39
Mentawai	Indonesia	$\delta^{18}O$	-4.00	97.92	12	Y	1858	1998	0.36	0.44	0.29	0.31	0.34	40
Bunaken	Indonesia	$\delta^{18}O$	1.87	123.00	12	Y	1860	1990	0.44	0.26	0.35	0.58	0.50	33
Rarotonga	Cook Islands	$\delta^{18}O$	-21.04	200.86	8	Y	1874	2000	0.45	0.29	0.25	0.44	0.46	29
Ningaloo Reef	Australia	$\delta^{18}O$	-21.15	112.84	6	Y	1879	1995	0.19	0.33	0.34	0.24	0.23	41
Madang	Papua New Guinea	$\delta^{18}O$	-5.04	144.86	4	Y	1880	1993	0.34	0.28	0.51	0.49	0.22	42
Laing	Papua New Guinea	$\delta^{18}O$	-4.03	143.85	4	Y	1884	1993	0.42	0.39	0.56	0.61	0.34	42
Palmyra Atoll	USA Territory	Sr/Ca	4.86	197.98	12	Y	1886	1998	0.59	0.53	0.54	0.72	0.63	43
Clipperton Atoll	France Territory	$\delta^{18}O$	9.95	250.96	12	Y	1893	1994	0.39	0.24	0.31	0.53	0.45	44
Tarawa Atoll	Rep. of Kiribati	$\delta^{18}O$	1.00	172.00	12	Y	1893	1989	0.64	0.61	0.54	0.65	0.71	45
Nauru	Rep. of Nauru	$\delta^{18}O$	-0.14	166.00	8	N	1897	1995	0.63	0.48	0.50	0.60	0.56	46

Table S3. Local coral correlation with SST and SSS. Absolute correlations between sea surface temperatures and sea surface salinity at each of the proxy site locations (500km radius) during the instrumental period (1920-1984) are reported for seasonal means (Ann) and for each single season MAM, JJA, SON and DJF, respectively. Interannual reported climate signal for all sites is given based on the references (Ref). Highlighted in bold is the dominate reported climate variable (SST and/or SSS and/or ENSO including precipitation).

Site Name	Proxy	Correlations (SST/SSS)					Reported	Ref
		Ann	MAM	JJA	SON	DJF	interannual signal	
Palmyra Atoll	$\delta^{18}O$	0.75/0.24	0.65/0.29	0.66/0.11	0.80/0.31	0.76/0.35	**SST**, SSS, **ENSO**	[28]
Savusavu Bay	$\delta^{18}O$	0.45/0.34	0.37/0.33	0.51/0.28	0.57/0.24	0.36/0.38	SST, **SSS**, **ENSO**	[29]
New Caledonia	Sr/Ca	0.55/0.09	0.41/0.24	0.58/0.14	0.63/0.10	0.56/0.19	**SST**, **ENSO**	[30]
New Caledonia	$\delta^{18}O$	0.22/0.17	0.32/0.27	0.25/0.19	0.22/0.17	0.09/0.24	**SST**, **ENSO**	[31]
Secas Island	$\delta^{18}O$	0.24/0.10	0.15/0.24	0.20/0.09	0.18/0.09	0.12/0.14	**SSS**, **ENSO**	[32]
Rarotonga	Sr/Ca	0.45/0.14	0.33/0.14	0.31/0.10	0.37/0.08	0.33/0.09	**SST**, **ENSO**	[29]
Rarotonga	$\delta^{18}O$	0.39/0.11	0.36/0.25	0.34/0.23	0.48/0.12	0.35/0.10	SST, **SSS**, **ENSO**	[29]
Savusavu Bay	Sr/Ca	0.36/0.10	0.23/0.12	0.35/0.10	0.41/0.21	0.34/0.20	**SST**, **ENSO**	[29]
Savusavu Bay	$\delta^{18}O$	0.33/0.10	0.34/0.12	0.39/0.10	0.44/0.21	0.44/0.20	SST, SSS, **ENSO**	[29]
Lombok	$\delta^{18}O$	0.15/0.17	0.12/0.09	0.45/0.14	0.33/0.18	0.25/0.21	**SST**, **ENSO**	[33]
Bali	$\delta^{18}O$	0.15/0.16	0.13/0.12	0.44/0.12	0.31/0.18	0.26/0.22	**SST**, **ENSO**	[33]
Double Reef	$\delta^{18}O$	0.38/0.55	0.49/0.53	0.18/0.34	0.25/0.46	0.45/0.54	SST, SSS, **ENSO**	[34]
Palau	$\delta^{18}O$	0.39/0.52	0.47/0.52	0.18/0.48	0.30/0.49	0.50/0.51	SST, SSS, **ENSO**	[35]
Clarion Island	$\delta^{18}O$	0.08/0.12	0.10/0.08	0.11/0.10	0.15/0.11	0.19/0.11	SST, SSS, **ENSO**	[36]
Maiana Atoll	$\delta^{18}O$	0.67/0.38	0.53/0.13	0.42/0.26	0.55/0.38	0.62/0.39	**SST**, SSS, **ENSO**	[37]
Vanuatu	$\delta^{18}O$	0.27/0.49	0.21/0.53	0.36/0.47	0.38/0.52	0.34/0.51	SST, SSS, **ENSO**	[38]
Tonga	$\delta^{18}O$	0.43/0.30	0.29/0.21	0.34/0.18	0.47/0.20	0.32/0.25	SST, SSS, **ENSO**	[39]
Mentawai	$\delta^{18}O$	0.36/0.14	0.44/0.11	0.27/0.09	0.31/0.15	0.34/0.16	**SST**, **ENSO**	[40]
Bunaken	$\delta^{18}O$	0.44/0.26	0.26/0.33	0.35/0.13	0.58/0.19	0.50/0.24	**SST**, **ENSO**	[33]
Rarotonga	$\delta^{18}O$	0.45/0.18	0.29/0.28	0.25/0.20	0.44/0.19	0.46/0.30	SST, **SSS**, **ENSO**	[29]
Ningaloo Reef	$\delta^{18}O$	0.19/0.13	0.33/0.13	0.34/0.19	0.26/0.18	0.24/0.16	**SST**, **ENSO**	[41]
Madang	$\delta^{18}O$	0.34/0.10	0.28/0.05	0.51/0.09	0.49/0.10	0.22/0.21	SST, SSS, **ENSO**	[42]
Laing	$\delta^{18}O$	0.42/0.19	0.39/0.14	0.56/0.06	0.61/0.17	0.34/0.18	SST, SSS, **ENSO**	[42]
Palmyra Atoll	Sr/Ca	0.59/0.09	0.53/0.16	0.54/0.15	0.72/0.25	0.63/0.24	**SST**, **ENSO**	[43]
Clipperton Atoll	$\delta^{18}O$	0.39/0.23	0.24/0.28	0.31/0.19	0.53/0.12	0.45/0.24	SST, SSS, **ENSO**	[44]
Tarawa Atoll	$\delta^{18}O$	0.64/0.34	0.61/0.19	0.54/0.26	0.65/0.35	0.71/0.38	SST, **SSS**, **ENSO**	[45]
Nauru	$\delta^{18}O$	0.63/0.43	0.48/0.23	0.50/0.46	0.60/0.49	0.56/0.37	**SST**, **ENSO**	[46]

Table S4. Correlations and source of individual records. Correlations for each record during its overlapping period (1920-1984) are listed with the NWP and NCT index, Niño3 and Niño 4 index, Trans Niño index (TNI), Multivariate ENSO index (MEI) and El Niño Modoki index (EMI). The dataset URL is also given.

Site Name	Correlations					URL
	NWP/NCT	Nino4/Nino3	TNI	MEI	EMI	
Palmyra Atoll $\delta^{18}O$	0.65/ 0.69	0.84/ 0.77	-0.42	0.79	0.65	https://www.ncdc.noaa.gov/paleo/study/1875
Savusavu Bay	-0.42/-0.51	-0.58/-0.56	0.18	-0.63	-0.38	https://www.ncdc.noaa.gov/paleo/study/16216
New Caledonia Sr/Ca	-0.34/-0.47	-0.50/-0.51	0.26	-0.52	-0.45	ftp://ftp.ncdc.noaa.gov/pub/data/paleo/coral/west_pacific/amedee2012.txt
New Caledonia $\delta^{18}O$	-0.24/-0.23	-0.31/-0.26	0.13	-0.28	-0.27	https://www.ncdc.noaa.gov/paleo/study/1843
Secas Island	-0.07/ 0.37	0.15/ 0.33	0.11	0.26	-0.02	https://www.ncdc.noaa.gov/cdo/f?p=519:1:::::P1_STUDY_ID:1853
Rarotonga Sr/Ca	-0.36/-0.47	-0.50/-0.50	0.13	-0.52	-0.27	ftp://ftp.ncdc.noaa.gov/pub/data/paleo/coral/east_pacific/rarotonga2006.txt
Rarotonga $\delta^{18}O$	-0.33/-0.52	-0.47/-0.53	0.10	-0.56	-0.26	ftp://ftp.ncdc.noaa.gov/pub/data/paleo/coral/east_pacific/rarotonga2006.txt
Savusavu Bay Sr/Ca	-0.44/-0.36	-0.49/-0.41	0.36	-0.47	-0.43	ftp://ftp.ncdc.noaa.gov/pub/data/paleo/coral/west_pacific/linsley2006/linsley2006-1f.txt
Savusavu Bay $\delta^{18}O$	-0.53/-0.28	-0.51/-0.36	0.44	-0.47	-0.49	ftp://ftp.ncdc.noaa.gov/pub/data/paleo/coral/west_pacific/linsley2006/linsley2006-1f.txt
Lombok	-0.33/-0.53	-0.50/-0.54	0.16	-0.57	-0.31	https://www.ncdc.noaa.gov/paleo/study/1903
Bali	-0.31/-0.54	-0.49/-0.55	0.15	-0.57	-0.28	ftp://ftp.ncdc.noaa.gov/pub/data/paleo/coral/west_pacific/bali2003.txt
Double Reef	-0.02/-0.34	-0.19/-0.32	-0.18	-0.31	0.04	ftp://ftp.ncdc.noaa.gov/pub/data/paleo/coral/west_pacific/guam2005.txt
Palau	-0.14/-0.64	-0.41/-0.61	-0.11	-0.57	-0.10	https://www.ncdc.noaa.gov/paleo/study/16339
Clarion Island	-0.00/ 0.07	0.05/ 0.07	-0.02	0.09	0.07	https://www.ncdc.noaa.gov/paleo/study/21310
Maiana Atoll	0.54/ 0.77	0.75/ 0.80	-0.35	0.78	0.55	https://www.ncdc.noaa.gov/paleo/study/1859
Vanuatu	-0.29/-0.39	-0.41/-0.41	0.07	-0.48	-0.22	https://www.ncdc.noaa.gov/paleo/study/13439
Tonga	-0.28/-0.48	-0.45/-0.50	0.05	-0.56	-0.24	https://www.ncdc.noaa.gov/paleo/study/6216
Mentawai	0.35/-0.13	0.16/-0.06	-0.38	0.06	0.32	ftp://ftp.ncdc.noaa.gov/pub/data/paleo/coral/indian_ocean/mentawai2008.txt
Bunaken	-0.48/-0.67	-0.67/-0.70	0.24	-0.73	-0.50	ftp://ftp.ncdc.noaa.gov/pub/data/paleo/coral/west_pacific/bunaken2003.txt
Rarotonga	-0.26/-0.60	-0.51/-0.60	0.00	-0.63	-0.24	ftp://ftp.ncdc.noaa.gov/pub/data/paleo/coral/east_pacific/rarotonga2006.txt
Ningaloo Reef	-0.29/-0.12	-0.27/-0.17	0.31	-0.24	-0.36	https://www.ncdc.noaa.gov/paleo/study/1867
Madang	-0.18/-0.65	-0.43/-0.62	-0.00	-0.56	-0.20	https://www.ncdc.noaa.gov/paleo/study/1866
Laing	-0.10/-0.62	-0.38/-0.59	-0.06	-0.52	-0.19	https://www.ncdc.noaa.gov/cdo/f?p=519:1:0:::P1_study_id:1866
Palmyra Atoll Sr/Ca	0.56/ 0.56	0.71/ 0.62	-0.39	0.67	0.61	https://www.ncdc.noaa.gov/cdo/f?p=519:1:0:::P1_STUDY_ID:10374
Clipperton Atoll	0.44/ 0.44	0.52/ 0.48	-0.33	0.51	0.51	https://www.ncdc.noaa.gov/paleo-search/study/17380
Tarawa Atoll	0.63/ 0.65	0.76/ 0.71	-0.39	0.76	0.57	https://www.ncdc.noaa.gov/cdo/f?p=519:1:::::P1_STUDY_ID:1916
Nauru	0.73/ 0.63	0.82/ 0.71	-0.61	0.80	0.72	http://hurricane.ncdc.noaa.gov/pls/paleox/f?p=519:1:4072198051706172::::P1_STUDY_ID:1842

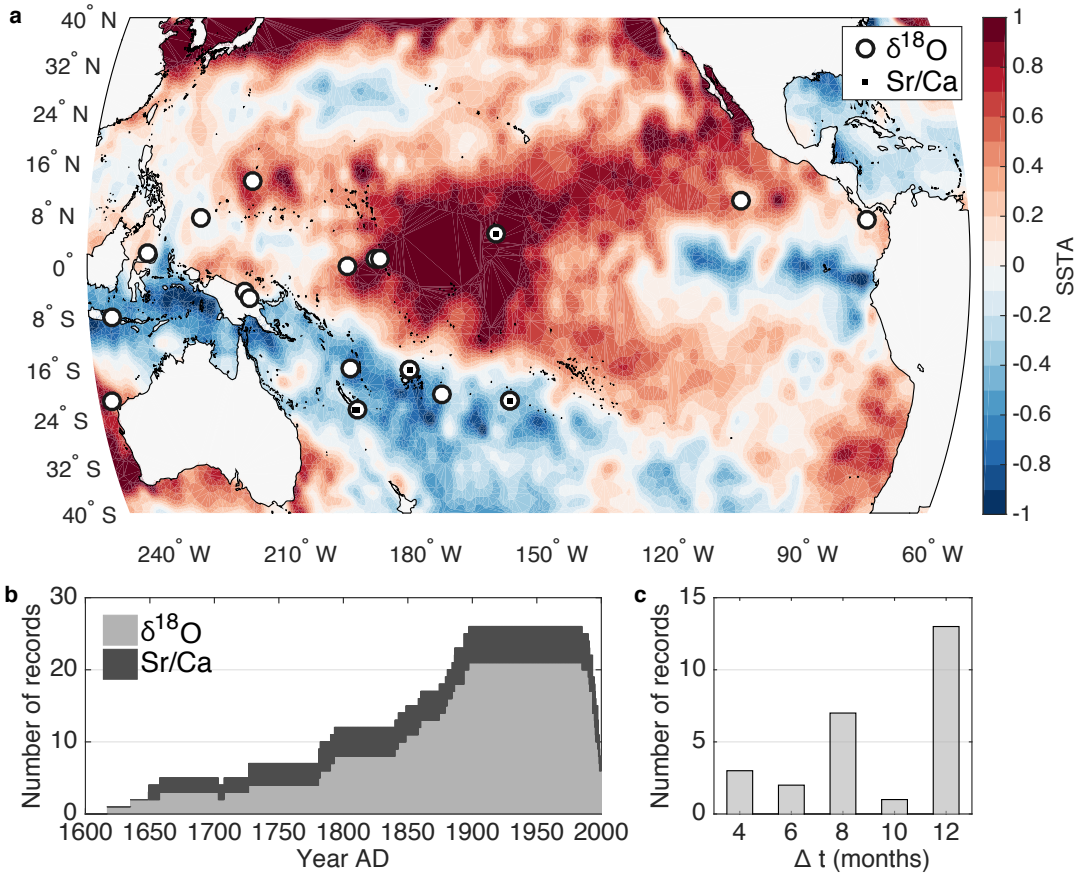

Figure S11. Paleoclimate coral network and spatiotemporal characteristics. **a,** Spatial distribution of proxy sites displayed on SST field typical for central Pacific El Niño (August 2004). **b,** Proxy availability during the period 1600-2000 **c,** Temporal resolution of the coral network represented by time steps per year.

3.3 Impact of pre-processing on results

3.3.1 Dating uncertainty

We test the impact of resampling the coral records to four samples a year (section 3.2). We apply a weighted average procedure to the records that aims to account for intraannual dating uncertainties within the records, which inevitably introduces some degree of smoothing of the data, but on the other hand removes some noise inherent in the coral records. To examine the sensitivity of the influence of the subsampling procedure (TableS5), we increase and decrease our uncertainty window over which a weighting of 0.5 is applied. The reconstructions show only minor differences in reconstruction variance with increasing or decreasing length of the smoothing window. However, the smoothing does impact identifying CP and EP events using the decision tree classification. The weighting procedure has an influence on the seasonal signatures and therefore the event classification itself (Table S5).

The classification of EP El Niño events is more robust against changes of the window width than the identification of CP events. Accounting for up to 2 months, does not change the detectability of EP events. Greater anomalies in °C in the case of EP El Niño events could be more robust, even if dating uncertainties are dismissed. For CP El Niño events, of generally smaller SSTA's, an optimal window width is found at 2 months (86%). These two months are in line with studies which quantify intra-annual coral dating uncertainties of about +/- 56 days [28;47]. This 2 month uncertainty range appears to be optimal in terms of detecting EP and CP El Niño events and might indicate a sufficient balance between the averaging smoothing signals, but also reducing noise in the coral records.

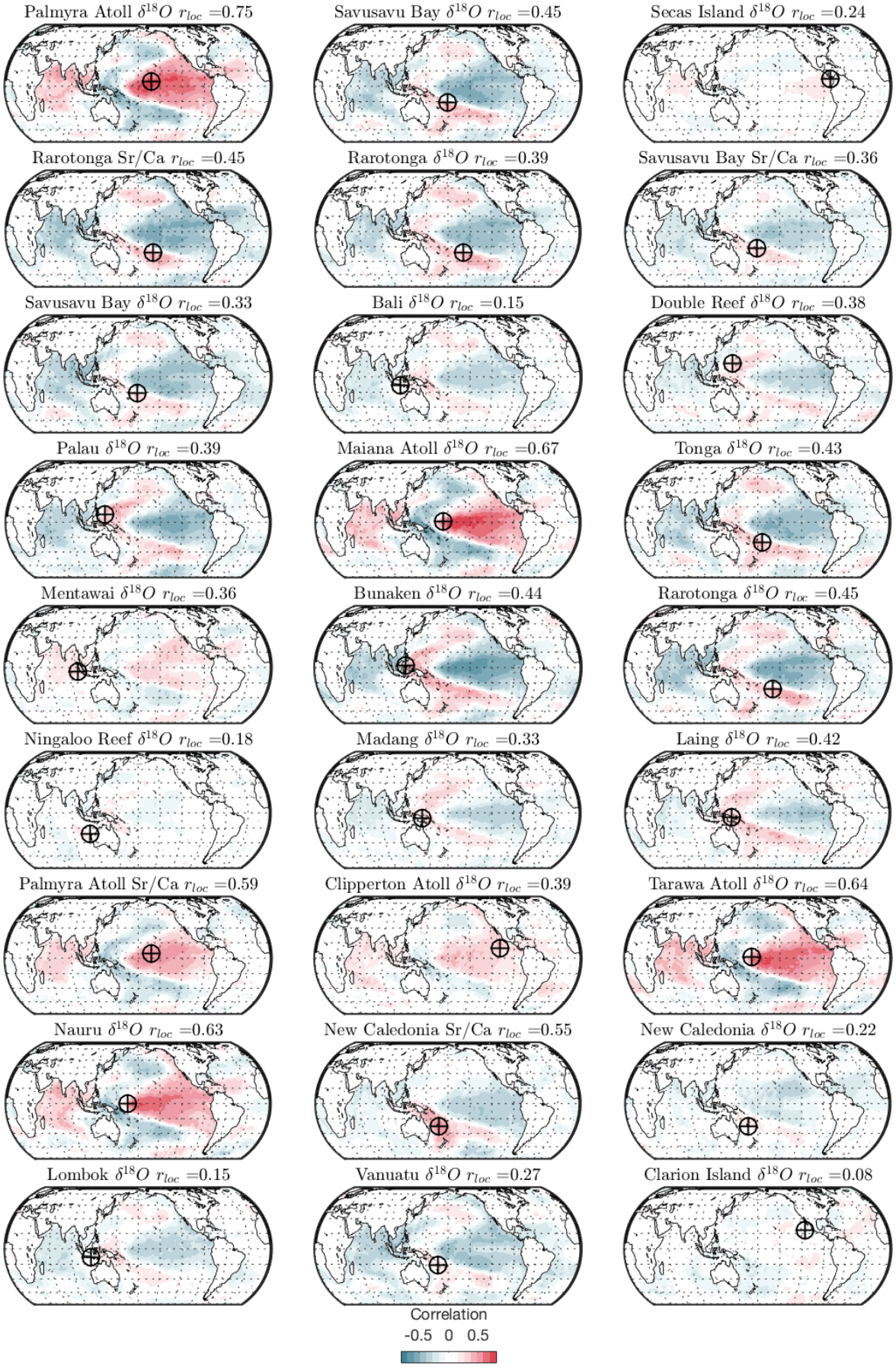

Figure S12. Spatial correlation of coral records with SST. Spatial correlations of each proxy records with gridded SSTA (HadISST) during 1920-1984. Local correlations r_{loc} refer to the maximum absolute correlation with SST close to the proxy site (500km). For visualisation purposes absolute correlations are given.

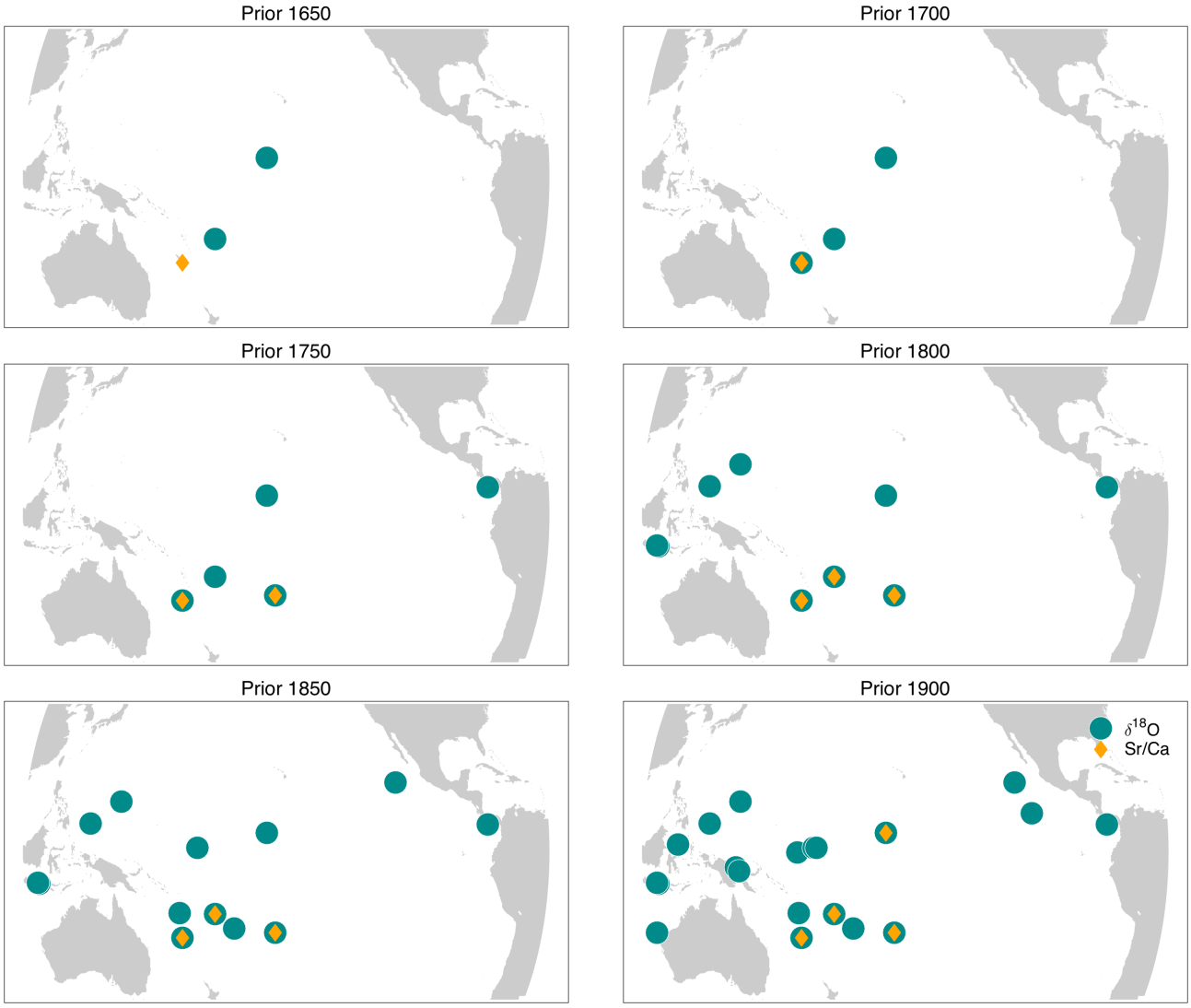

Figure S13. Coral record availability back in time. Spatial distribution of seasonally resolved coral records differentiated for $\delta^{18}O$ and Sr/Ca records back in time. Note that some sites are in close proximity.

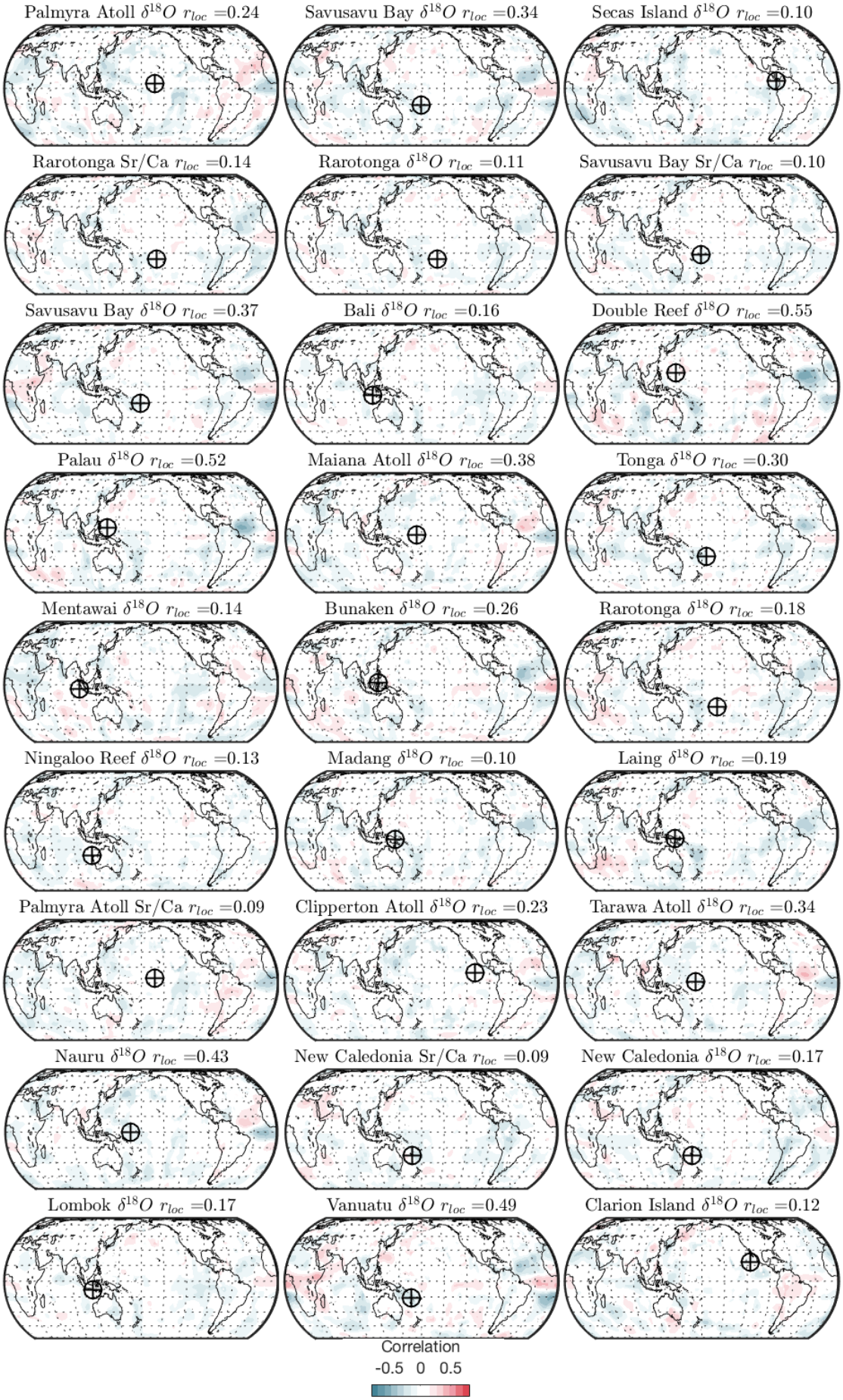

Figure S14. Spatial correlation of coral records with SSS. Spatial correlations of each proxy records with gridded sea surface saliniy (SSS Had EN4.2.0 dataset) [14] during 1920-1984. Local correlations r_{loc} refer to the maximum absolute correlation with SSS close to the proxy site (500km). For visualisation purposes absolute correlations are given.

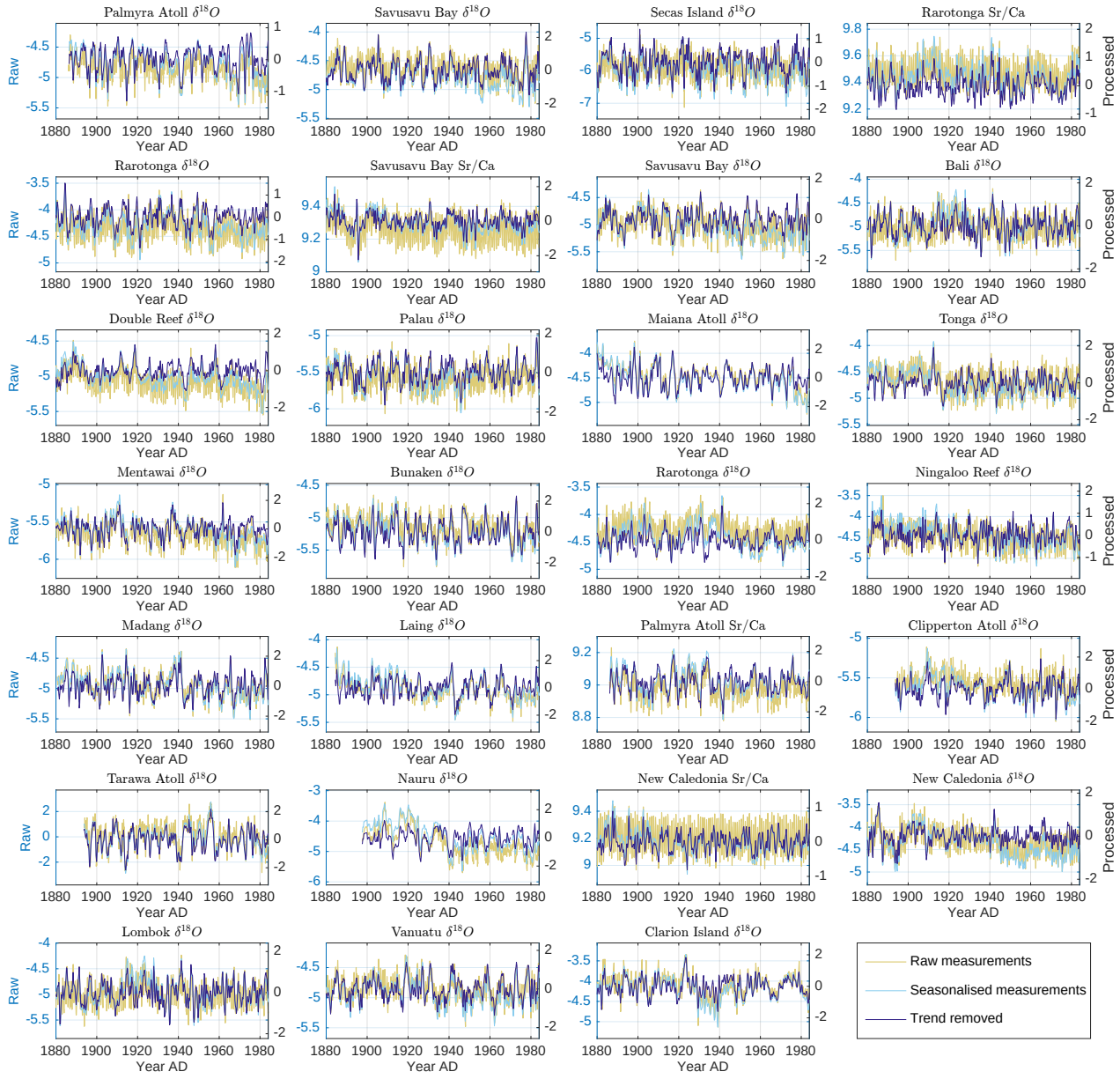

Figure S15. Pre-processing of coral data. Time series of individual records showing the raw data (left y-axis) and the processed time series (right y-axis). Raw y-axis refers to coral $\delta^{18}O$ in [‰] and Sr/Ca records in [mmol/mol].

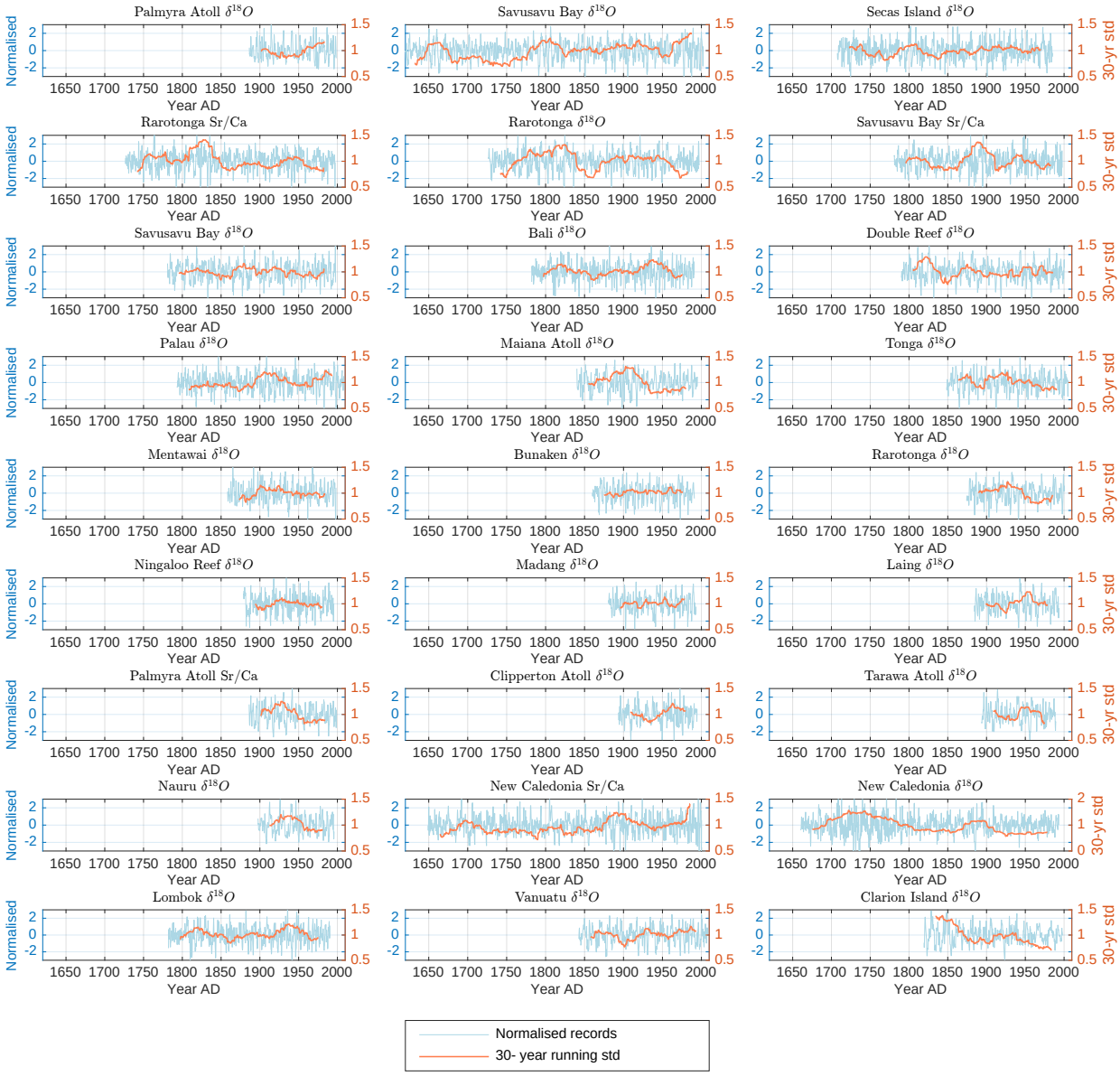

Figure S16. Normalised coral data. Time series of normalised records (left y-axis) and time series as a 30-yr moving standard deviation (right y-axis).

3.3.2 Chronological uncertainty

Table S5. Dating uncertainty. Detection of EP and CP El Niño years during the instrumental period based on varying uncertainty window width used to seasonalise the coral records.

Window width (months)	% of EP El Niños identified	% of CP El Niños identified
0	87.5	64.3
1	87.5	64.3
2	**87.5**	**85.7**
3	75	28
5	75	14

While intra-annual dating uncertainties were considered by applying a weighted average procedure to the records, age uncertainties related to missing, false or double counted years are also conceivable[47]. There are ways to minimise the age model uncertainties. For instance, our reconstruction is derived from multiple coral records, which minimises the influence of individual age uncertainties in single records[48;49].
The impact of these chronological uncertainties on our results is difficult to quantify since these errors occur randomly, in particular prior to the instrumental period when tie point matching to the instrumental data is not possible. However, chronological uncertainty gains importance if only a single record is considered. Combining coral records from multiple locations often helps to mitigate these uncertainties[48;50]. Sensitivity studies to dating errors, quantified by 10 years for old coral records, have shown that the majority of variance is retained since not all records show a dating offset[50]. Within our methodological framework, we use the common signal from an entire coral network using principal components. In principle, these leading components represent the largest shared variance. We retain only the first principal components that account for 80% of the total variance as possible predictors to avoid possible co-linearity effects and remove non-climate related noise.
Considering that single records can have age errors, we test this sensitivity by leave-one-out analysis (Figure S17) and leaving randomly individual years out (Fig. S19). Correlation analysis between the reduced network and the reconstruction based on the entire network shows some differences between NCT and NWP, but highlights strong resemblance (Figure S17). The NCT reconstruction is sensitive to the exclusion of the Sr/Ca record from New Caledonia, whereas the NWP reconstruction shows strongest sensitivities to the $\delta^{18}O$ record from New Caledonia and Palmyra Atoll.

The majority of records show enhanced variability from 1880 onwards, reduced variability from around 1820-1880 (expect for Clarion Island) and relative high variability from 1780-1820 (Figure S19 a,). Prior to 1780, variability for most of the records is reduced except for New Caledonia $\delta^{18}O$ record. The overall changes in variance are a common feature in the majority of records. We test the possibility that records dropping in and out are causing changes in variance by only considering 4 records. Figure S19 b shows the interquartile range for the moving variance derived from only 4 records at a time. Until 1740, the interquartile range shows similar behaviour and independent of which records are available. Prior to 1740, the inclusion of individual records can influence the variance. The limited number of records increases the uncertainty around the variance. Given the possibility that age uncertainties could potentially influence the absolute variance, we the variance structure by leaving individual years out (S19 c,). Considering different error rates (25%, 20%, 10%, 5% and 1%), we test the sensitivity of overall variance to possible dating uncertainties. An error rate of 25% represents for example that 25% of the individual years are incorrect and have been removed. Reduced variance prior to 1880 remains a common feature despite missing data of a maximum 25% error rate. Differences of variance are again strongest in the early 17th century due to the limited number of records.

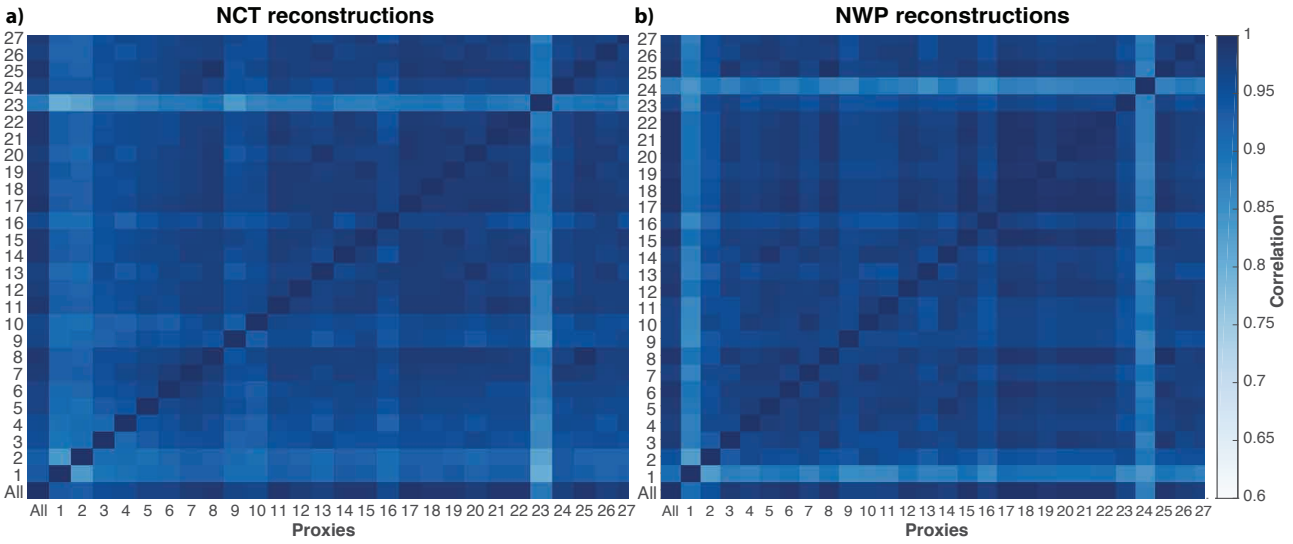

Figure S17. Influence of individual records. Comparison between the different NCT (**a**) and NWP (**b**) index reconstructions based on exclusion of individual records. The first entry includes all coral records whereas the following 1-28 entries are reconstructed indices based on all records except the indicated one. The correlations are for the overlapping reconstructed periods. 1: Palmyra Atoll $\delta^{18}O$, 2: Savusavu Bay, 3: Secas Island, 4: Rarotonga Sr/Ca, 5: Rarotonga $\delta^{18}O$, 6: Savusavu Bay Sr/Ca, 7: Savusavu Bay $\delta^{18}O$, 8: Bali, 9: Double Reef, 10: Palau, 11: Maiana Atoll, 12: Tonga, 13: Mentawai, 14: Bunaken, 15: Rarotonga, 16: Ningaloo Reef, 17: Madang, 18: Laing, 19: Palmyra Atoll Sr/Ca, 20: Clipperton Atoll, 21: Tarawa Atoll, 22: Nauru, 23: New Caledonia Sr/Ca, 24: New Caledonia $\delta^{18}O$, 25: Lombok, 26: Vanuatu, 27: Clarion Island

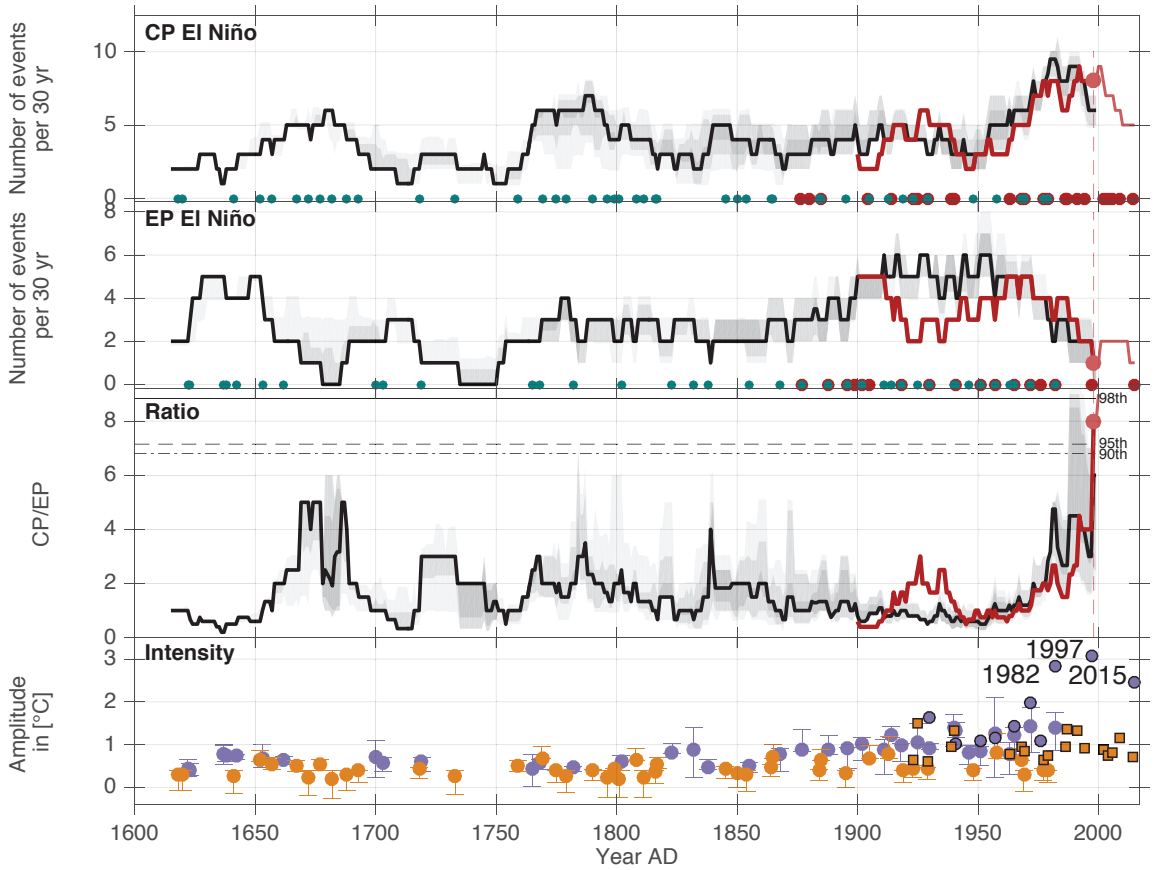

Figure S18. Reconstruction sensitivity to leaving out individual records. Number of CP El Niño events (**a**), EP El Niño events (**b**) and ratio of CP to EP events (**c**) and intensity (**d**) in sliding 30-yr windows; instrumental (red), bootstrapped median (black) and uncertainty range in grey shadings (75^{th}, 90^{th}, 95^{th} percentiles) shown. The uncertainty range is based on the reconstructions from leave-one-out analysis.

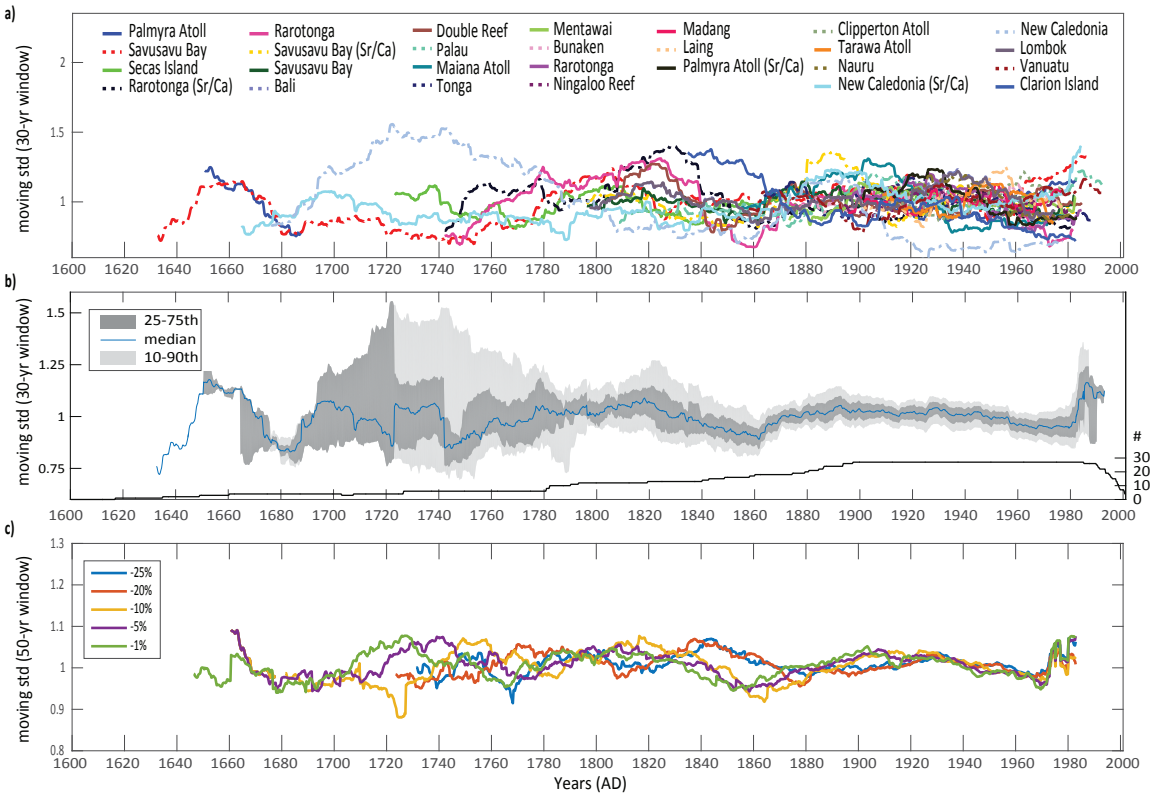

Figure S19. Variability and sensitivity of variance. Moving standard deviation of normalised individual records (**a**), interquartile range of moving standard devaition of any possible combination (17750) of 4 proxy records (**b**) and moving standard deviation of proxy records by leaving data out (**c**). The age error rate corresponds to overall 25%, 20%, 10%, 5% and 1% of the data randomly left out.

3.3.3 Impact of detrending

A spline filter with a cut-off frequency of 150 years is applied to remove 50% of variance associated with multi-centennial variability similarly to ref.[51]. The choice to detrend the records stems from several aspects. Our primary interest is to preserve high-frequency variability in the coral records, independently from low-frequency fluctuations and trends. Although low-frequency variability like the Interdecadal Pacific Oscillation (IPO)[52;53] is often hypothesised to affect El Niño[54;55], its underlying physical mechanism in conjunction with mean state changes and anthropogenic forcing are not fully understood[56]. By focusing on the seasonal differences itself, we circumvent these possible associated impacts. Moreover, our understanding of multi-centennial trends in the coral records itself is limited, particularly for low-frequency variations in $\delta^{18}O$[51;57;58].

We examine the impact of low-frequency trends in the records on the reconstructions and El Niño amplitudes (Figure S20). The influence of removing trends in the coral records prior to the reconstruction is most obvious from around 1700-1780. During this period the NCT index reconstruction shows strong low-frequency variability resulting in cooler than normal SST's compared to adjacent time periods. For the NWP reconstruction, the removal of trends seems to enhance the variability during this time period, but is not associated with changes of the mean-state in terms of SST. These observations agree with results based on the annual coral records shown by ref.[51].

The differences in terms of El Niño amplitudes are less affected by coral detrending (Figure S20c,d). Most of the El Niño events show similar maximum amplitudes in the Niño 3 and Niño 4 region compared to our reconstruction. Only a few event years exceed the error bar estimation, including the early CP year 1652 and 1918/1919. Interestingly, 1918/1919 shows less warming in the instrumental records than suggested by the nondetrended reconstruction. Moreover, being classified as a central Pacific El Niño event could explain why

the El Niño year 1918/1919 has been ranked as a weak event[31] although some coral-based studies suggested a strong event[59]. Removing low-frequency variability prior to the reconstruction emphasises the high-frequency bands that are important for our classification approach, results in higher validation statistics and removes the possibility of over-interpretation of less-well understood low-frequency information recorded by coral records.

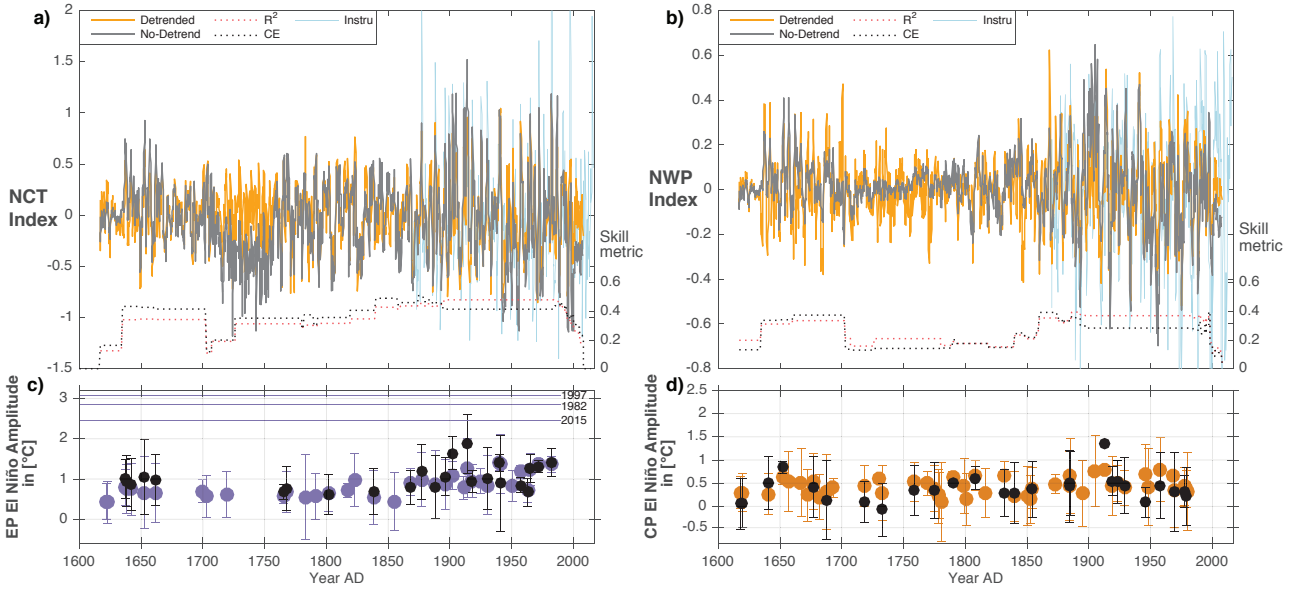

Figure S20. Influence of coral detrending. Comparison between NCT (**a**) and NWP (**b**) index reconstructions from detrended and non-detrended records and the instrumental record (Instru), including skill metrics on secondary axis (non-detrended). Event amplitudes for EP (**c**) and CP El Niño events (**d**) are compared based on the detrended records (coloured) and non-detrended records (black). Error bars indicate 95% confidence interval from bootstrapping.

4 El Niño diversity and its fingerprints on the coral records

4.1 El Niño diversity across nests

The seasonally resolved coral network consists of records covering different time periods. The common period covered by all records (full network) extends from 1897-1984. A two-way nested procedure is applied to account for varying network sizes back and forward in time. The main paper results are based on the full network. We test all nests in terms of each single PC's contribution towards a specific type of El Niño by correlation analysis (Supplementary Fig. S21). The two types of El Niño resemble the first and second PC of the full proxy network as Eastern and Central Pacific El Niño variability in terms of the temporal and spatial pattern derived from correlation analysis. The first principal component derived from various nests shows invariably significant correlations with the first instrumental EOF. Across all nests the main common signal is expressed by the first PC and related to the Eastern Pacific-type El Niños. In contrast, the second EOF of SSTA in the Pacific is mainly correlated with nests' second PC's but also exhibits significant correlations on subsequent PCs. It follows that the variability of Central Pacific El Niño can't be fully explained by a single PC and rather multiple PCs, depending on the specific nest (see Fig. S23). Given the differences among the nests, we use multiple PCs that account for up to 80% explained variance for our reconstruction.

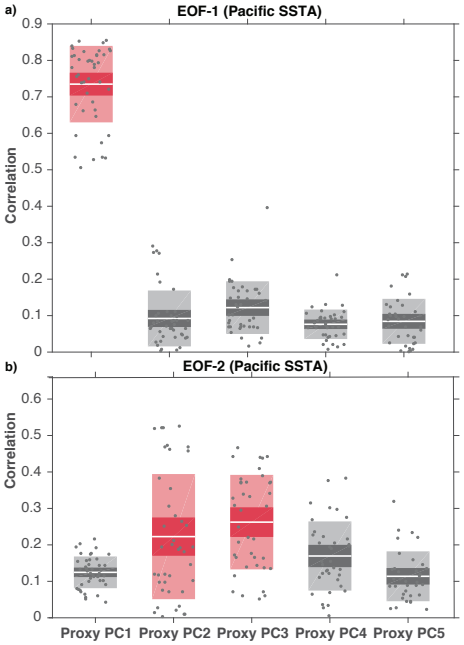

Figure S21. Correlations between principal components of proxy nests and instrumental principal components. Distributions of correlation coefficients (absolute) between EOF-1 (**a**) and EOF-2 (**b**) based on the instrumental SSTs in the Pacific and each principal component of the proxy nests. Significant correlations (median, $p < 0.01$) are highlighted in red.

4.2 El Niño diversity and regression pattern

The spatial pattern of SSTs associated with the EOF modes derived from the coral network bears a strong resemblance with the EP and CP El Niño pattern derived from the observations. This pattern is robust across different seasons. Figure 1 shows the regression pattern for JJA as one example. Supplementary Figure S22 shows the seasonal evolution for the two EOF patterns. The spatial pattern of the proxy EOF modes are similar to those represented by the SST observations. The EP pattern shows pronounced warming near the South American coast, extending westwards. This instrumental pattern has a strong resemblance to the leading mode of the coral network for all seasons. The coral network also captures the EP dipole pattern, primarily because there is a strong negative contribution from coral sites in the western Pacific region. The zonal tripolar pattern associated with CP El Niño events is apparent across the seasons but most distinctly visible during JJA. Later in the year, the SST across the Pacific shows a slight warming also in the Eastern Pacific, which results in less distinct tripolar pattern during DJF.

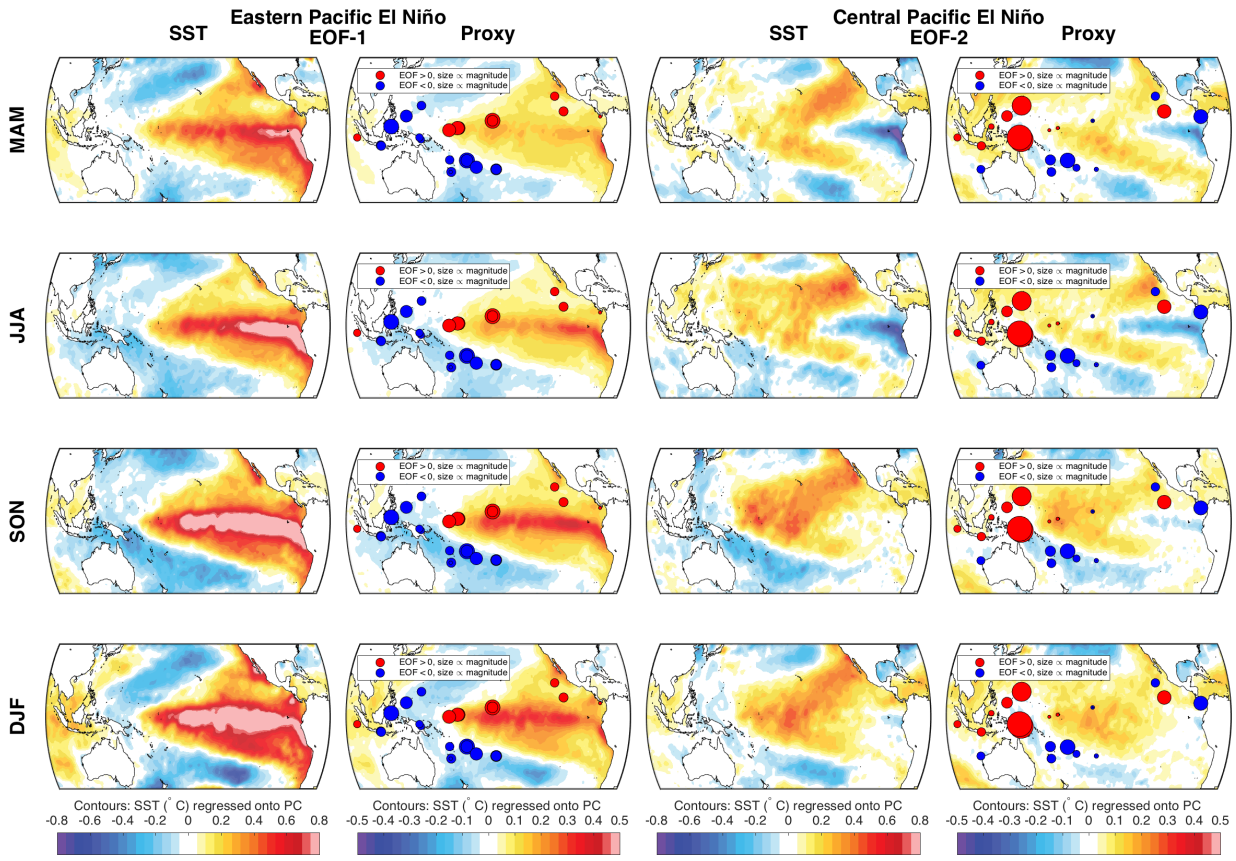

Figure S22. El Niño diversity in instrumental and coral data. First and second EOF modes of seasonal instrumental SSTA (HadISST) in the tropical Pacific (140°E-80°W, 30°S-30°N) regressed onto different seasonal SSTA (row 1: MAM, row 2: JJA, row 3: SON, row 4: DJF). Same for the coral network EOF-modes regressed onto SSTA during corresponding seasons and coral site loadings. (Similar to Figure 1 in the main paper).

4.3 Seasonal distinction of EP and CP El Niño events

The seasonal evolution of CP and EP events in the instrumental records shows significant differences during the developing and peak phase. The temporal evolution of the NWP index, which mainly reflects CP variability, shows that SSTAs in CP events are higher in boreal summer and autumn (JJA-SON) and a divergence between CP and EP in DJF. The second EOF of the coral network shows a similar seasonal evolution to instrumental temperatures in the warm pool. During the developing and peak phases, the coral network shows anomalously warmer conditions during CP years compared to EP years. Main Figure 2 shows in comparison the evolution of SST during the EP and CP years as recorded by the NCT index (a) and the first coral EOF (c). The instrumental data and the coral data show similar seasonal warming during EP and CP events. The NCT index shows a significantly stronger warming during EP events than CP events. Both El Niño types show peak warming during SON-DJF. A similar seasonal evolution to the instrumental NCT index is recorded by the first EOF of the coral network. The seasonality of the coral records as shown by the principal components does not exactly correspond with the instrumental indices but shows in general a similar seasonal evolution.

5 Seasonal reconstruction

5.1 Diverse network - common ENSO signal

The seasonal coral network aggregates a number of different records that are unified by a common ENSO signal. Nevertheless, the network includes different time periods covered and information from different locations (5.1.1) as well as different measurements (5.1.2). The impact of these differences are individually examined in the following section.

5.1.1 Records from different locations covering different periods

The leading patterns of tropical SST variability in the Pacific are closely related to the dominant co-varying signals across the entire coral network expressed the two leading EOFs (Fig 1, & Supplementary Fig. S22). The coral network combines different sites from various regions across the Pacific that are influenced by ENSO conditions. Given these differences, we follow ref. [50] and assess the impact of individual regions.

1. **High CC:** high correlation between Niño3.4 SSTA and $\delta^{18}O$ (here "CC" refers to "correlation coefficient"). This subset includes Savusavu, Palmyra, Kiritimati, and Vanuatu (Malo Channel).
2. **East/Central:** directly influenced by the equatorial cold tongue in the eastern/central Pacific. This subset includes Clipperton, Secas, Palmyra, and Kiritimati.
3. **SPCZ:** locations directly influenced by the South Pacific Convergence Zone. This subset includes Vanuatu (both sites), Savusavu, New Caledonia, and Rarotonga.
4. **Warm Pool:** locations in the western Pacific warm pool. This subset includes Tarawa, Maiana, Laing, Madang, Nauru, and Bunaken.

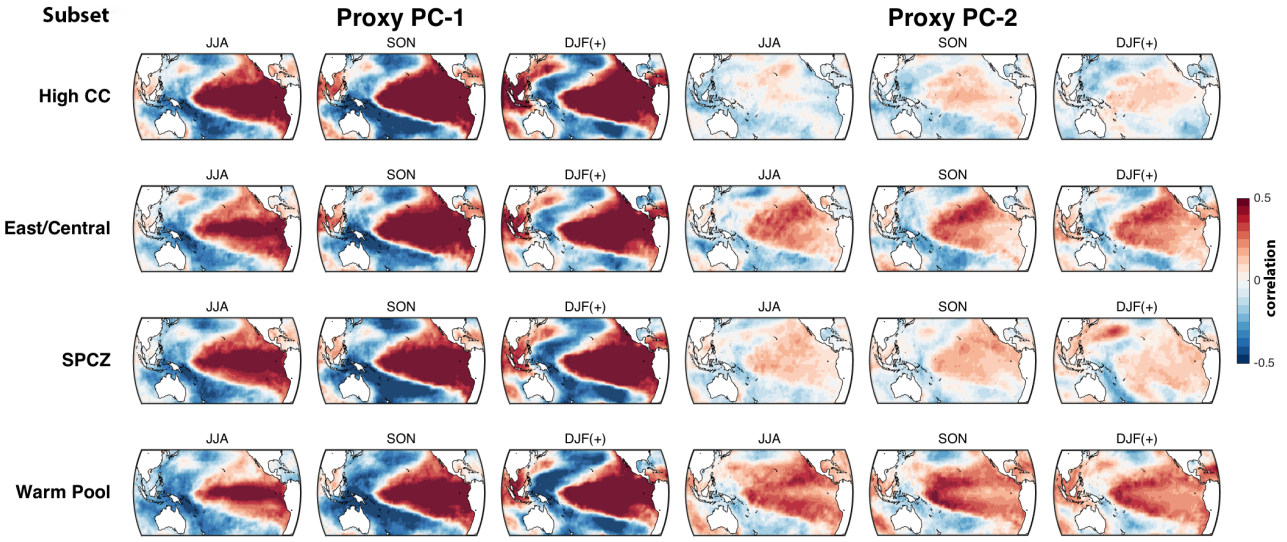

Figure S23. Sensitivity to site selection. Seasonal correlations of Proxy PC-1 and PC-2 dervied from subsets of records from different regions with gridded SST HadISST during the instrumental period (1950-1984).

The coral records from different regions (including ENSO-peripheral regions, Supplementary Fig. S23) detect some of the main EP and CP El Niño SST patterns. Similarly to ref. [50] sites from off-equatorial regions like the SPCZ show a greater sensitivity to CP type events. The inclusion of coral data from El Niño peripheral regions

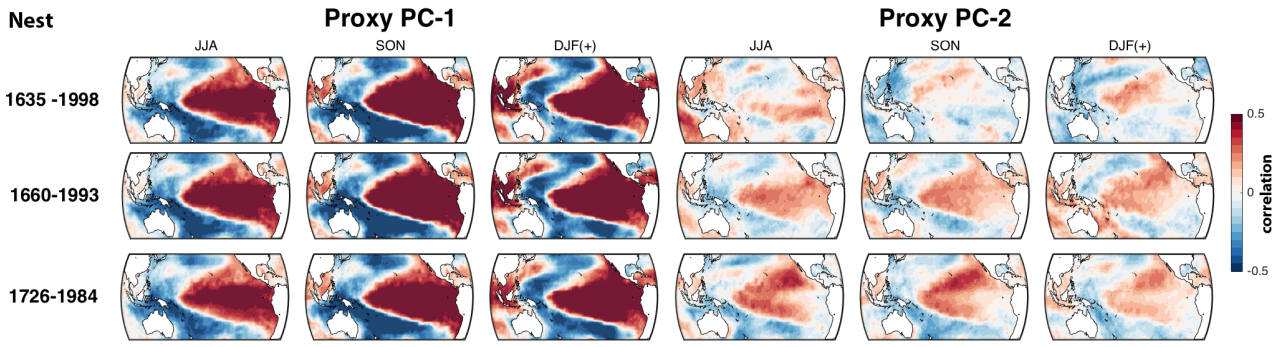

Figure S24. ENSO pattern in early nests. Seasonal correlations of Proxy PC-1 and PC-2 dervied from different nests with gridded SST HadISST during the instrumental period (1950-1984).

improves the number of reconstructed large-scale SST modes[60]. These are influenced downstream by local meteorological conditions as shown by the composite Figs with precipitation and temperature (Supplementary Fig. S7 & S8). The coral records from off-equatorial regions make significant contributions to the reconstruction skill.

The coral records that cover early time periods (Supplementary Fig. S24) detect the main CP and EP El Niño SST patterns using as few as 2-4 records. This is consistent with results by ref.[50] and ref.[48]. The EP El Niño fingerprint remains strongest on the first principal component of the proxy network. Nonetheless, a correlation is still apparent for the second PC. The reconstruction greatly benefits from the diversity of sites, regions and records.

5.1.2 Sensitivity to Sr/Ca records

The multi-proxy coral network includes 23 $\delta^{18}O$ records as well as 4 records based on Sr/Ca. Whereas $\delta^{18}O$ is dependent on SST and the $\delta^{18}O$ of seawater (see section 3.1.1), Sr/Ca ratios are viewed as being primarily driven by SST variability[61;62]. We examine the influence and relative contribution of Sr/Ca records on our reconstruction. Based on the limited number of Sr/Ca records, we can deduce its impact by excluding these records and compare our results to a reconstruction based on $\delta^{18}O$ records only (Figure S25). The influence of Sr/Ca ratios on our reconstruction is very limited and only notable for the NCT reconstruction. Moving correlations indicate that the contributions from the Sr/Ca records alter the NCT reconstruction most notably from 1700-1870. The NWP reconstruction is mostly unaffected, expect for a brief period of enhanced variability from 1820-1880. There is no obvious direct impact of Sr/Ca records on the event amplitudes. Deviations of EP and CP El Niño amplitude vary within the given error estimates. We conclude that Sr/Ca can potentially amplify reconstructed SST variability, in particular during low-variability periods inferred by the $\delta^{18}O$ records. A reverse implication of this could indicate that reduced variance based on $\delta^{18}O$ records is not likely solely driven by SST variability and could originate from the $\delta^{18}O$ of seawater. The exclusion of Sr/Ca records does not alter the frequency or amplitudes of EP and CP El Niño events.

Furthermore, we examine the role of $\delta^{18}O$ in coral records that is not predominately driven by SST variability but seawater salinity. At an annual time scale, three $\delta^{18}O$ records (Savusavu Bay, Secas Island and Tarawa Atoll) are reported to be predominately driven by SSS variability. In addition to these sites, the records from Vanuatu, Double Reef and Palau show higher correlations with SSS variability than SST variability. By excluding these records from the reconstruction, we examine the influence of a mixed signal of SSS and SST on $\delta^{18}O$ in the coral records (Figure S26). Without these 6 records, the variance of the NCT reconstruction is slightly reduced compared to the full network reconstruction. The inclusion of salinity sensitive $\delta^{18}O$ records appears to slightly enhance the reconstructed amplitudes of the NCT reconstruction (Figure S26,c). The NWP reconstructions show no noticeable difference in terms of variance (Figure S26,d). The intensity of EP and CP events shows little difference between the different sets of proxies (Figure S26,e,f). The influence of salinity on

the reconstructed variance and intensity of events is relatively small.

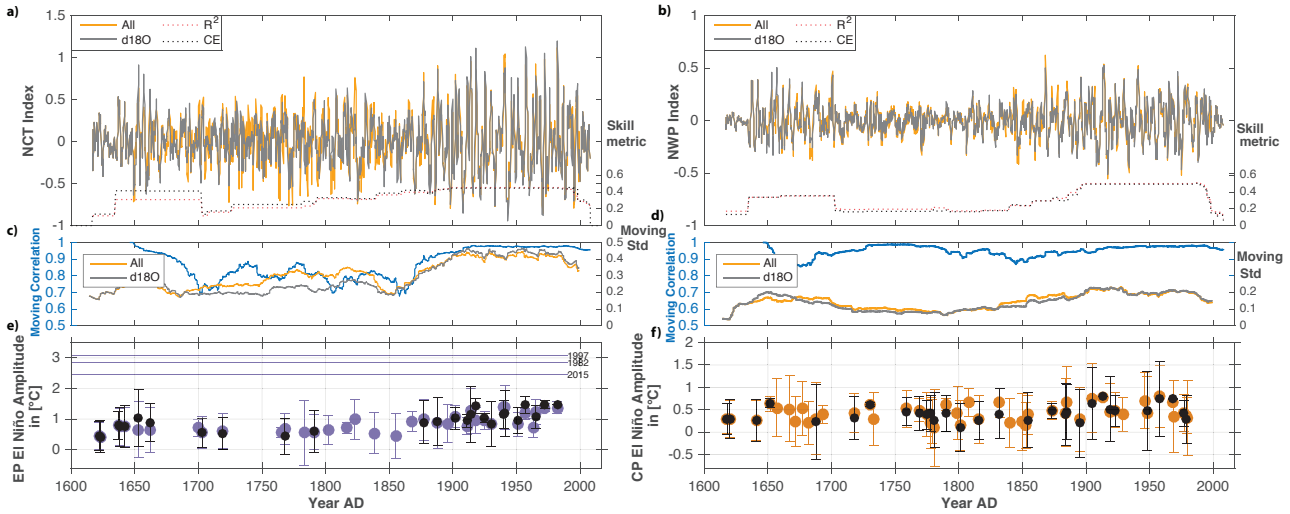

Figure S25. Sensitivity to Sr/Ca. Comparison between the different the NCT (**a**) and NWP (**b**) index reconstructions based on all records and $\delta^{18}O$ records only, including skill metrics on secondary axis ($\delta^{18}O$ records only). **c,d** Moving correlations of 30 year windows between the original reconstruction and the $\delta^{18}O$ only reconstruction (left axis). Moving standard deviations are shown on the right secondary axis. Event amplitudes for EP (**e**) and CP El Niño events (**f**) are compared for reconstructions using all records (colored) and $\delta^{18}O$ records only (black). Error bars indicate 95% confidence interval from bootstrapping.

5.1.3 Influence of varying nests

The different time periods covered by the coral records require a nested approach which concatenates reconstructions derived of different sets of proxy records. We examine the influence of the nested approach on our reconstruction by comparing the reconstruction to a "fixed-nest" reconstruction. A fixed-nest refers to a set of proxies that cover the same period. The nest #7 starting in 1726 (see Table S6) includes 6 proxy records (Figure S27). The fixed nest reconstructions based on 6 proxy records explains less variance for NCT ($R^2 = 0.29$) and NWP ($R^2 = 0.22$) indices compared to the stiched original reconstructions. The variance of the fixed nest NCT reconstruction is smaller compared to the original reconstruction, but larger uncertainty range. The fixed nest reconstructions show similar periods of reduced variance in the early 18th and mid 19th century. The fixed nest NWP reconstruction shows similar periods of reduced variance as the NCT reconstruction when only a fixed set of proxies is being used. The NWP reconstruction based on the fixed nest appears to reconstruct more variance in the early 18th century and less variance from 1825 onwards compared to the full-nest reconstruction.

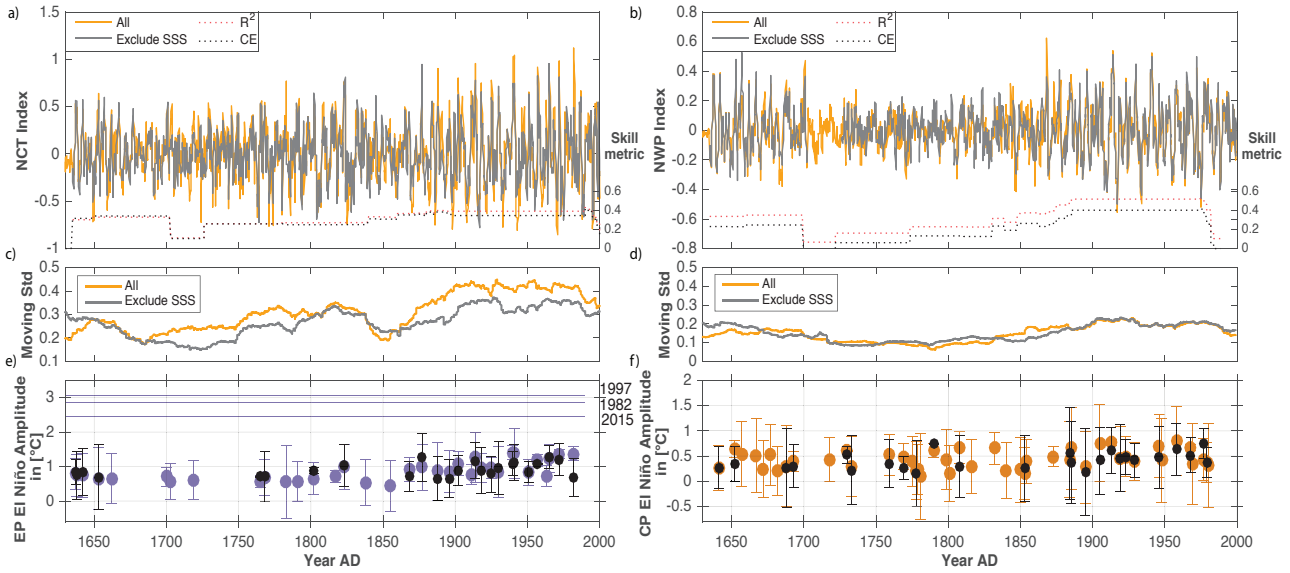

Figure S26. Sensitivity to salinity. Comparison between the different the NCT (**a**) and NWP (**b**) index reconstructions based on all records and excluding 6 $\delta^{18}O$ records (Savusavu Bay, Secas Island, Tarawa Atoll,Vanuatu, Double Reef, Palau) that may not predominantly driven by SST variability but salinity or a mixed signal, including skill metrics on secondary axis ($\delta^{18}O$). **c,d** Moving standard deviations of original and the subset of excluding possible salinity ($\delta^{18}O$ records only). Event amplitudes for EP (**e**) and CP El Niño events (**f**) are compared for reconstructions using all records (colored) and $\delta^{18}O$ subset only (black). Error bars indicate 95% confidence interval from bootstrapping.

5.2 Seasonal Reconstruction

5.2.1 Method

We employ a nested, Principal Component Regression (PCR) approach using variational Bayesian inference [63;64] to reconstruct the seasonal NCT and NWP indices. The seasonally resolved coral network consists of records covering different time periods (see Table S6). The common period covered by all coral records (full network) extends from 1897-1984. We use a nested approach to maximise the length of our reconstruction. Based on the availability of the records (Table S6), we build subsets (nests) of records that are first decomposed into their leading components using Principal Component Analysis (PCA). We then regress the leading n PCs against the NCT and NWP target indices. If the set of PCs for each nest of proxy records is $X = \{x_1, x_2, .., x_n\}$, the predictors, a multiple regression model for a target index with dependent variable $Y = \{y_1, y_2, .., y_n\}$, regression coefficients $\beta = \{\beta_1, \beta_2, .., \beta_n\}$ and noise ϵ is formulated as: $Y = X\beta + \epsilon$.

The regression coefficients β are traditionally obtained by least-squares estimation or maximum likelihood fitting of the probability distributions from a frequentist approach, assuming X does not provide information about the conditional distribution of Y given X [65]. We employ here a Bayesian approach which derives the regression coefficients from the posterior probability distribution by variational inference. For further details about regression using variational Bayesian inference, see refs. [64;66–68].

We then develop continuous index reconstructions by merging the results of each regression. For each nest, the reconstruction is adjusted to have a common mean and standard deviation with the most replicated nest. The final continuous reconstruction is created by splicing the nests of reconstructions together. Where more than one nest covers the same period we splice the nest with maximum time-integrated RE (Eq. 4). Our PCR approach using variational Bayesian inference yields similar results to a classical PCR approach, but with higher explained variance (Fig. S28).

Table S6. Additional information on nests. Information on the different nests covering the entire period from 1617-2008, with the start and end years, the number of contributing records and the individual records are 1: Palmyra Atoll $\delta^{18}O$, 2: Savusavu Bay, 3: Secas Island, 4: Rarotonga Sr/Ca, 5: Rarotonga $\delta^{18}O$, 6: Savusavu Bay Sr/Ca, 7: Savusavu Bay d18O, 8: Bali,9: Double Reef,10: Palau, 11: Maiana Atoll, 12: Tonga, 13: Mentawai, 14: Bunaken, 15: Rarotonga,16: Ningaloo Reef, 17: Madang, 18: Laing, 19: Palmyra Atoll Sr/Ca, 20: Clipperton Atoll, 21: Tarawa Atoll, 22: Nauru, 23: New Caledonia Sr/Ca, 24: New Caledonia $\delta^{18}O$, 25: Lombok, 26: Vanuatu, 27: Clarion Island

Nest	Start Year	End Year	Total #	Records included in the nest
1	1617	2002	1	2
2	1635	1998	2	1 2
3	1649	1998	3	1 2 23
4	1660	1993	4	1 2 23 24
5	1660	1993	3	2 23 24
6	1707	1984	4	2 3 23 24
7	1726	1984	6	2 3 4 5 23 24
8	1780	1984	8	2 3 4 5 6 7 23 24
9	1782	1984	10	2 3 4 5 6 7 8 23 24 25
10	1790	1984	11	2 3 4 5 6 7 8 9 23 24 25
11	1793	1984	12	2 3 4 5 6 7 8 9 10 23 24 25
12	1819	1984	13	2 3 4 5 6 7 8 9 10 23 24 25 27
13	1840	1984	14	2 3 4 5 6 7 8 9 10 11 23 24 25 27
14	1842	1984	15	2 3 4 5 6 7 8 9 10 11 23 24 25 26 27
15	1848	1984	16	2 3 4 5 6 7 8 9 10 11 12 23 24 25 26 27
16	1858	1984	17	2 3 4 5 6 7 8 9 10 11 12 13 23 24 25 26 27
17	1860	1984	18	2 3 4 5 6 7 8 9 10 11 12 13 14 23 24 25 26 27
18	1874	1984	19	2 3 4 5 6 7 8 9 10 11 12 13 14 15 23 24 25 26 27
19	1879	1984	20	2 3 4 5 6 7 8 9 10 11 12 13 14 15 16 23 24 25 26 27
20	1880	1984	21	2 3 4 5 6 7 8 9 10 11 12 13 14 15 16 17 23 24 25 26 27
21	1884	1984	22	2 3 4 5 6 7 8 9 10 11 12 13 14 15 16 17 18 23 24 25 26 27
22	1886	1984	23	2 3 4 5 6 7 8 9 10 11 12 13 14 15 16 17 18 19 23 24 25 26 27
23	1886	1984	24	1 2 3 4 5 6 7 8 9 10 11 12 13 14 15 16 17 18 19 23 24 25 26 27
24	1893	1984	26	1 2 3 4 5 6 7 8 9 10 11 12 13 14 15 16 17 18 19 20 21 23 24 25 26 27
25	1897	1984	27	1 2 3 4 5 6 7 8 9 10 11 12 13 14 15 16 17 18 19 20 21 22 23 24 25 26 27
26	1897	1989	26	1 2 4 5 6 7 8 9 10 11 12 13 14 15 16 17 18 19 20 21 22 23 24 25 26 27
27	1897	1990	25	1 2 4 5 6 7 8 9 10 11 12 13 14 15 16 17 18 19 20 22 23 24 25 26 27
28	1897	1990	24	1 2 4 5 6 7 8 9 10 11 12 13 14 15 16 17 18 19 20 22 23 24 26 27
29	1897	1990	23	1 2 4 5 6 7 9 10 11 12 13 14 15 16 17 18 19 20 22 23 24 26 27
30	1897	1993	22	1 2 4 5 6 7 9 10 11 12 13 15 16 17 18 19 20 22 23 24 26 27
31	1897	1994	19	1 2 4 5 6 7 9 10 11 12 13 15 16 19 20 22 23 26 27
32	1897	1994	18	1 2 4 5 6 7 9 10 11 12 13 15 16 19 22 23 26 27
33	1897	1995	17	1 2 4 5 6 7 9 10 12 13 15 16 19 22 23 26 27
34	1897	1995	16	1 2 4 5 6 7 9 10 12 13 15 19 22 23 26 27
35	1886	1997	15	1 2 4 5 6 7 9 10 12 13 15 19 23 26 27
36	1886	1997	13	1 2 6 7 9 10 12 13 15 19 23 26 27
37	1886	1998	11	1 2 9 10 12 13 15 19 23 26 27
38	1886	1998	9	1 2 9 10 12 15 19 23 26
39	1886	1998	8	2 9 10 12 15 19 23 26
40	1874	2000	7	2 9 10 12 15 23 26
41	1874	2000	6	2 9 10 12 15 26
42	1848	2002	4	2 10 12 26
43	1848	2005	3	10 12 26
44	1842	2007	2	10 26
45	1793	2008	1	10

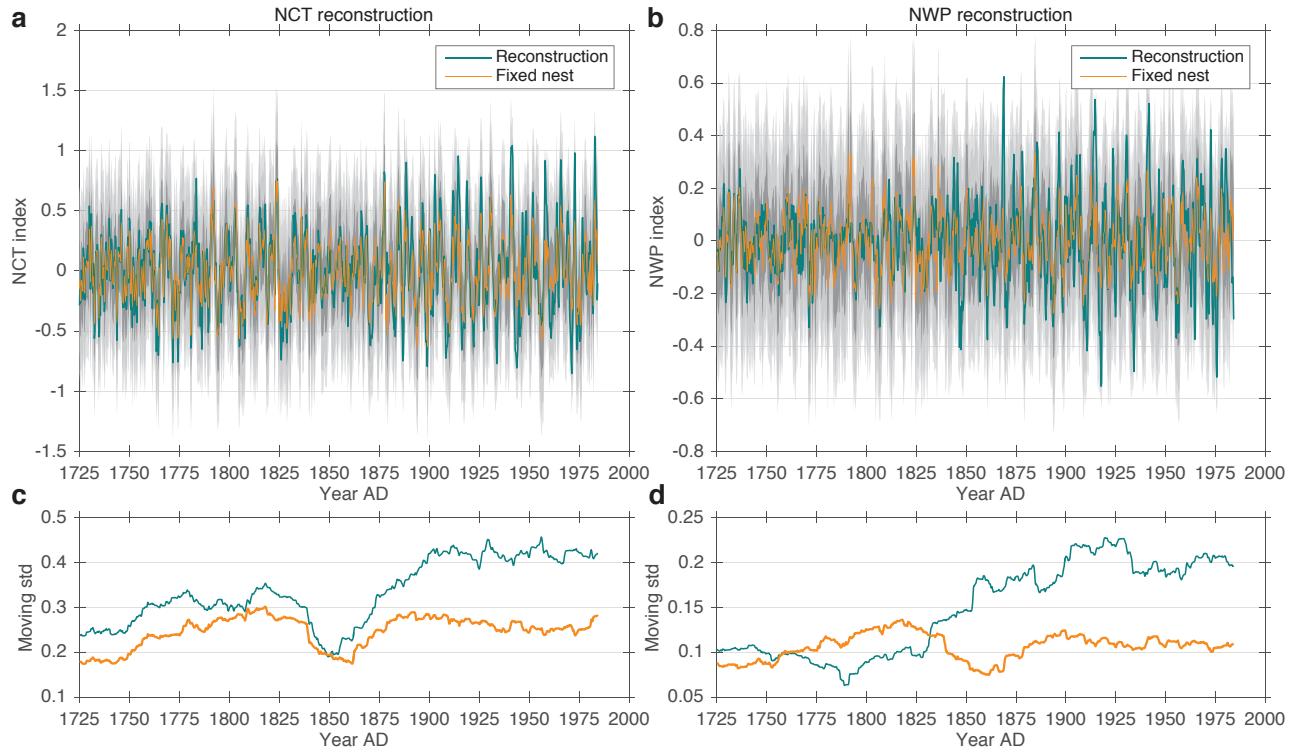

Figure S27. Influence of varying nests. Comparison of NCT (**a**) and NWP (**b**) index reconstructions from the stiched nested reconstruction (teal) and a set number of proxies starting in 1726 called a fixed nest (nest # 7) (yellow). Uncertainty range of the 95th percentiles in grey shadings correspond to the fixed nest reconstructions. Comparison of the moving standard deviations of 30 year windows for the fixed nest (yellow) and the stiched reconstruction (teal) of the NCT (**c**) and NCWP (**d**) reconstructions.

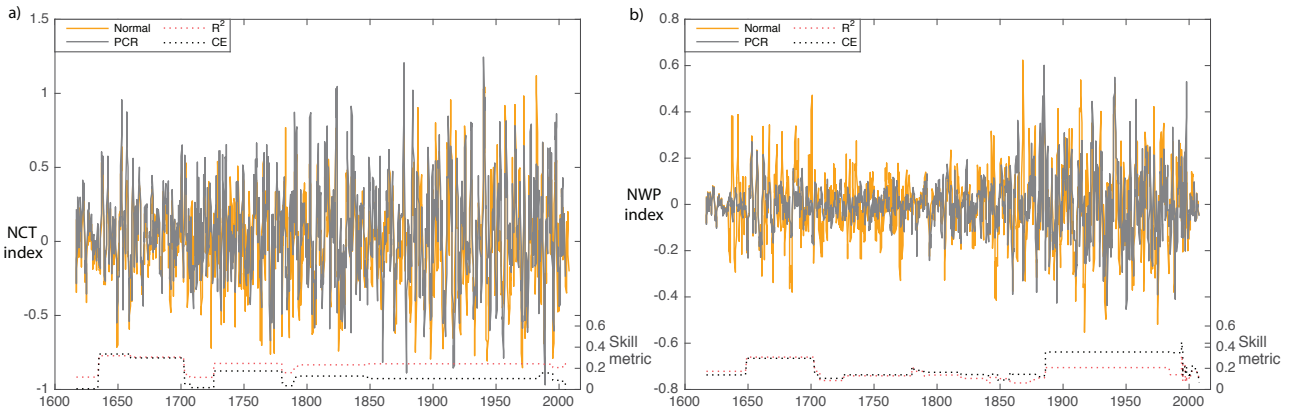

Figure S28. Influence of reconstruction method. Comparison of NCT (**a**) and NWP (**b**) index reconstructions from a classical principal regression approach (PCR) compared to our approach using variational Bayesian inference ('Normal'). Skill metrics on secondary (right side) axes refer to the classical regression approach.

5.2.2 Verification

The skill of the reconstruction is evaluated and tested by several statistical measures on an independent verification period. In order to verify the statistical model, which was fitted over the calibration period, Reduction of Error (RE) and the Coefficient of efficiency (CE) and the verification period square of the Pearson correlation ($VRSQ$) are used as metrics of verification skill. The coefficient of determination R^2 (R-*square* or RSQ) for verification $VRSQ$ and its equivalent for the calibration period ($CRSQ$) measure the common variance of

normally distributed time series and quantify the amount of variance explained by the reconstruction [69]:

$$R^2 = \frac{SSR}{SST} = \frac{\sum_{i=1}^{n} [\hat{y}(x_i) - \bar{y}]^2}{\sum_{i=1}^{n} (y_i - \bar{y})^2} \tag{3}$$

The coefficient of determination R^2 is the proportion of the regression sum of squares (SSR), which is the squared difference between the predicted values $\hat{y}(x)$ and the data mean of y and the total sum of squares (SST), which is the sum of squared deviations of y values and their mean $\bar{y}$. The R^2 can range between 0 (no linear relationship) and 1.0, which indicates a perfect linear fit of the predictors with the regression line [70].
The reduction of error (RE, Eq. 4) is a skill score which sets the reconstruction relative to the climatology variance as the reference. Positive values of RE indicate better performance of the regression model than using the climatological variance $MSE(\bar{y}_{cal})$, relative to the mean squared error ($MSE(\bar{y})$) of the measurement [71].

In theory RE has a range of (-infinity,+1] and in the case of an unbiased and reliable reconstruction, RE complies with the squared correlation of predictand and predictor [70].
The coefficient of efficiency (CE, Eq. 5) is similar to the RE in that it is related to the mean squared error ($MSE(\bar{y})$) of the reconstructed values, but its denominator is the mean and variance of the verification period $MSE(\bar{y}_{verf})$ instead of the climatological variance of the calibration period $MSE(\bar{y}_{cal})$. The CE has a range of (-infinity,+1] [72].

$$RE = 1 - \frac{MSE(\bar{y})}{MSE(\bar{y}_{cal})} \tag{4}$$

$$CE = 1 - \frac{MSE(\bar{y})}{MSE(\bar{y}_{verf})} \tag{5}$$

5.2.3 Error estimation

The reconstructed indices represent 50% and 56% of the observed variance of NCT and NWP during the common period (1920-1984) respectively (Fig.3). We model the reconstruction error that remains unexplained using autoregressive (AR) modelling. The SST observations and reconstruction in the Pacific have a statistically significant autocorrelation of up to four seasons (Figure S29). An estimate of the confidence level is obtained with a bootstrap approach by adding 1000 realisations of autoregressive AR(4) noise (four seasons). The regression-based uncertainties are estimated from the autoregressive covariance structure of the residuals in the verification period.

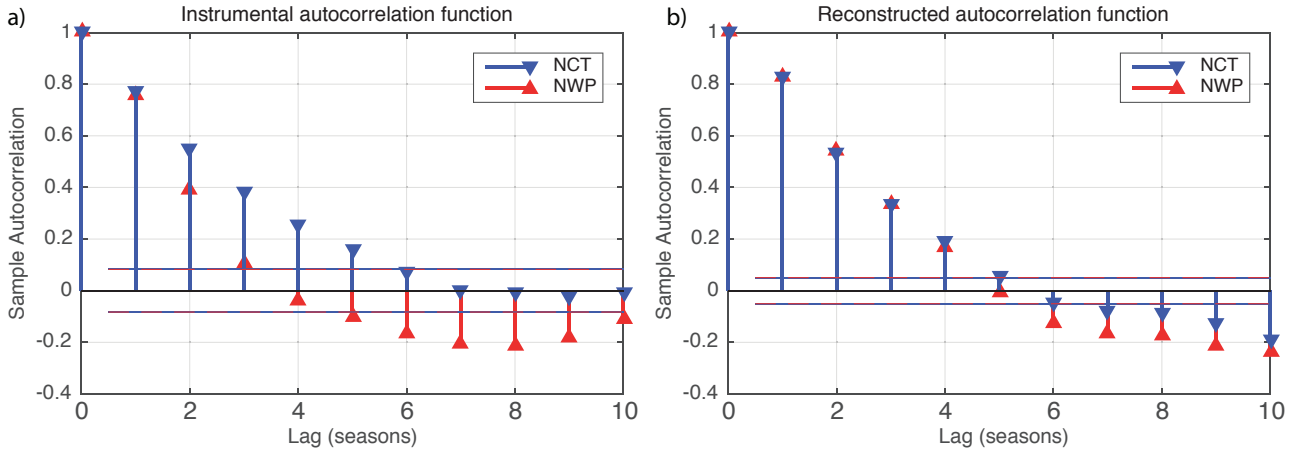

Figure S29. Autoregressive properties of NWP & NCT. Instrumental (**a**) and reconstructed (**b**) autocorrelation functions up to lag 10. Lags are shown in season; a lag of 4 equals to 1 year.

5.2.4 Comparison with existing ENSO reconstructions

We assess the accuracy of our new index reconstruction by comparing it against existing ENSO reconstructions. The variance of the NWP and NCT reconstructions shows high variable phases, which might be related to either the declining number of available coral records or climatic related variance changes. We compare our variance evolution over time with existing reconstructions derived from various coral archives (Extended Fig.S30). The standard deviation in 31 year periods is compared for the past 400 years (after linear detrending). All reconstructions exhibit a decline in variance compared to the modern period. The variance is maximal during the instrumental period (1900 onwards), with the early and late part of the 20th century period showing the highest variability. The coral-derived reconstruction by ref.[73] has its maximum variance during the period from around 1800-1830 which is the coldest period according to the reconstruction. This increase in variance coincides with a brief period of increased variance in our Niño Cold Tongue reconstruction, while the Warm Pool reconstruction has below average variance. A number of the coral-derived reconstruction appear to agree on the early 18th century period of reduced variability. The period of noticeably reduced variance occurring in our Warm Pool reconstruction between 1720 and 1800 is also visible in other coral based reconstructions.

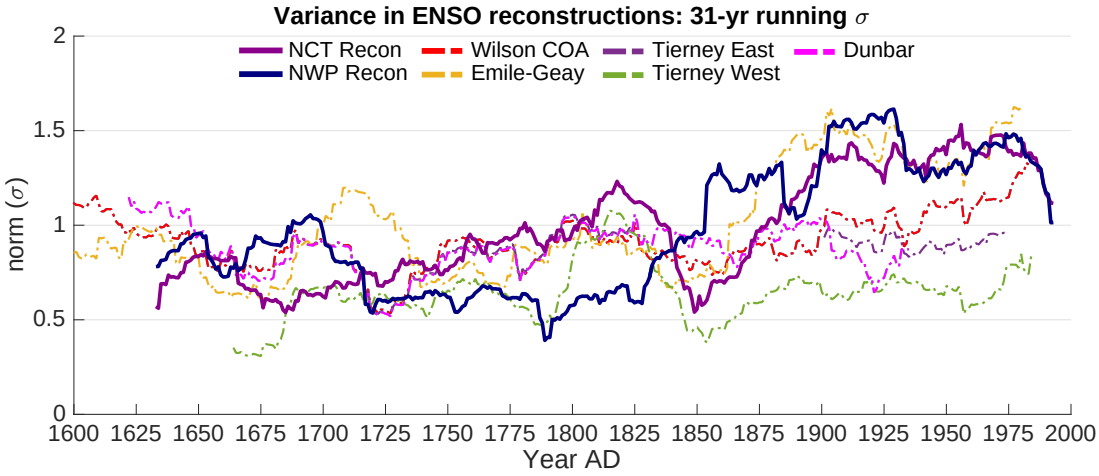

Figure S30. Variance in ENSO reconstructions. Evolution of variance presented by its normalised standard deviation aggregated over 31-year moving windows. The Niño Warm Pool (NWP) and Niño Cold Tongue (NCT) reconstructions are highlighted and compared to the coral based reconstructions: Wilson COA (Center of Action)[57], Emile-Geay[74], Tierney East and West[73], Dunbar[75].

5.2.5 Event amplitudes of EP and CP El Niño events

The instrumental indices as well as the index reconstructions of NWP and NCT allow to identify EP and CP events back in time and during the most recent period. Based on classified events, the maximum excursion of the indices can be reported as a reference about the El Niño event amplitude. Most commonly, the intensity of El Niño events is often reported as the maximum SSTA in the Niño3 region or the maximum Oceanic Niño index (ONI) (Supplementary Figure S31,f). The reconstruction measures the two types of El Niño is based on the Niño warm Pool index and the Niño cold tongue index, which are related to the SSTA in the Niño 3 and Niño 4 region (see section 2.1). By quantified the maximum amplitude of the indices, the reconstructed and instrumental indices indicate the intensity and type of El Niño events[76]. The amplitudes of the NCT index, related mainly to the EP El Niño type are larger compared to the NWP index. The intensity can be either represented by the indices itself as index units (e.g. Supplementary Figure S31,b) or back transformed into Niño 3 and Niño 4 sea surface anomalies in °C (Supplementary Figure S31,c,e). According to equation 1, the intensity of EP events is derived from the maximum amplitude in the Niño3 region, whereas the CP event amplitudes are derived from the Niño4 amplitudes during an El Niño event.

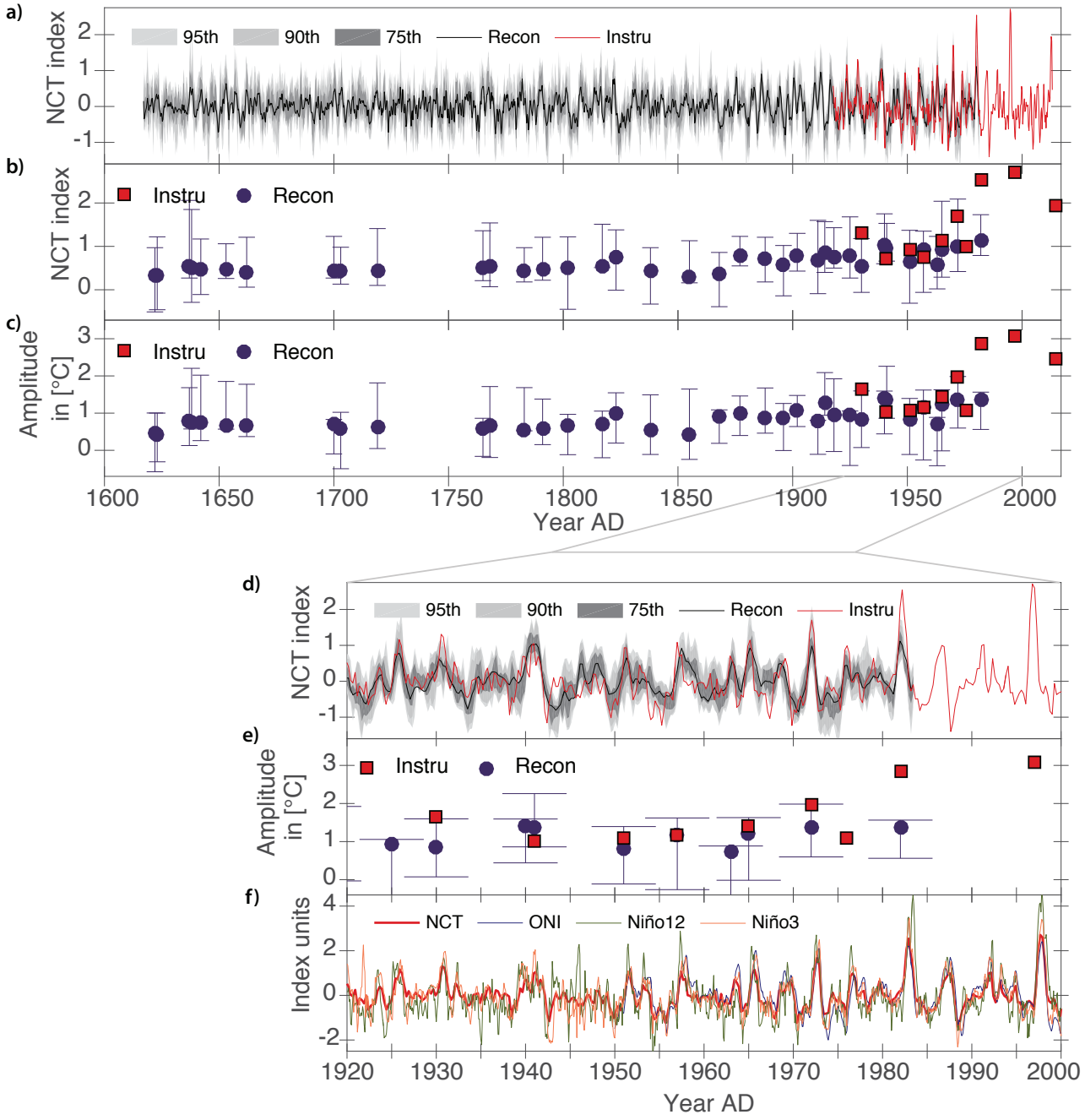

Figure S31. Event amplitude of EP events. NCT index reconstruction (black) with uncertanty range (grey shade) in comparison with the instrumental record (red) **a**. Identified EP El Niño events in the reconstruction (blue) with uncertanty range (bars) and the instrumental events (red) measured by the NCT index **b**. Same as **b** but ampltides are derived from maximum SST anomaly in Niño 3 and Niño 4 region **c**. **d,e** show details during the instrumental period and a comparision with alternative indices: Oceanic Niño index (ONI), Niño1.2 index and Niño3 regional averages **f**.

6 Classification of EP and CP El Niño and sensitivities

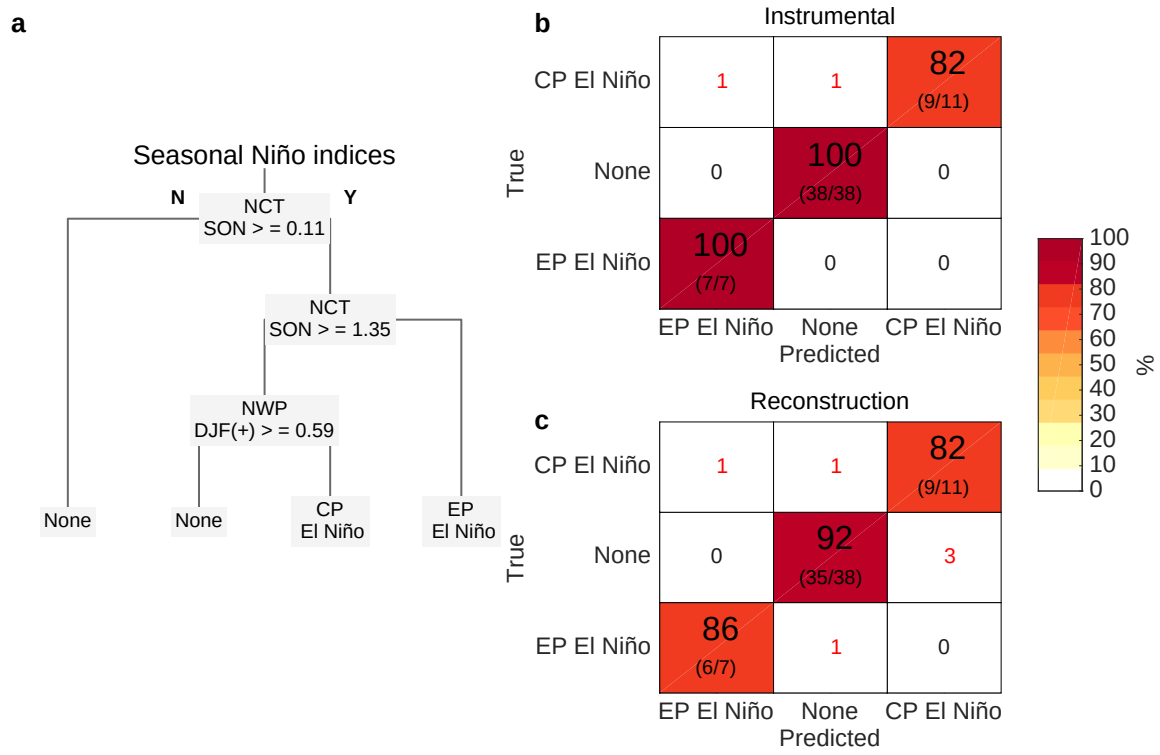

Figure S32. Classification tree of El Niño events. a, Decision tree based on the seasonal Niño indices (NWP and NCT) as predictor variables and three categories: EP El Niño, CP El Niño and neither event (none). Each branch indicates a decision (Y: satisfied condition (right), N: unsatisfied condition (left)) **b,** Confusion matrix as applied and trained on the instrumental data by the decision tree during the training period (1950-2005). **c,** Similarly, for the reconstruction during the training period (1950-2005). Entries in the confusion matrix give agreement in % with details about the number of events below (#predicted events/#actual events) and the number of missclassifications in red. This means, for the upper right square in b) and c), that 9 out of 11 (82%) of CP El Niño events where correctly classified.

Table S7. El Niño events of the past 400 years. El Niño events based on the reconstructions and instrumental data. Years in bold highlight events that are picked up by the reconstruction and the instrumental training data. In addition to the reconstruction, the decision tree has been applied to the latest period of instrumental data (1950-2015), for which the events years are given in italics.

EP El Niño events	CP El Niño events
1622, 1623, 1637, 1638, 1642, 1653, 1662	1618, 1620, 1641, 1652, 1657, 1667, 1672, 1677, 1682, 1688, 1693
1700, 1703, 1719, 1765, 1768, 1783, 1791	1718, 1730, 1733
1802, 1817, 1823, 1838, 1855, 1868, 1877, 1888, 1896	1759, 1769, 1775, 1778, 1779, 1781, 1790, 1799
1902, 1911, 1914, 1918, 1925, 1930, 1940, 1941	1801, 1808, 1816, 1832, 1840, 1850, 1853, 1854, 1873, 1884, 1885, 1895
1951, **1957**, 1963, **1965**, **1972**, **1982**, ***1997***	1905, 1913, 1919, 1923, 1929, 1946, 1948
2015	1958, **1968**, **1969**, **1977**, **1979**, 1980, ***1986***, ***1987***, ***1991***, ***1994*** ***2002***, ***2004***, *2006*, *2009*, *2014*

6.1 Evaluation of classification

The confusion matrix is a diagnostic tool to verify nonprobabilistic forecasts for discrete predictands. Applied to our classification, the possible discrete predictands are CP El Niño event, EP El Niño event or no event (None). The one-to-one correspondence between all the possible predictands and the observations can be displayed in a confusion matrix. A confusion matrix can also known as a contingency table. Equivalent to contingency tables, true positive (TP), true negative (TN), false positive (FP) and false negative (FN) quantities are reported (see Supplementary Fig. S32 b,c). The performance of our classification can then be evaluated with the help of the quantities reported by the confusion matrix (Supplementary Table S8). The following evaluation metrics are used and reported: accuracy (Eq. 6), precision (Eq. 7), sensitivity (Eq. 8), F-score (Eq. 9) and Matthews correlation coefficient (MCC Eq. 10) [77–79].

Table S8. Classification evaluation. Evaluation of decision tree based on the instrumental (Instru) and reconstructed time series (Recon) as classifiers using the accuracy, precision, sensitivity, F-score and Matthews correlation coefficient (MCC) metrics.

	Instru	Recon
Accuracy	0.976	0.929
Precision	0.964	0.893
Sensitivity	0.964	0.893
Fscore	0.964	0.893
MCC	0.946	0.839

$$\text{Accuracy: } ACC = \frac{TP + TN}{P + N} = \frac{TP + TN}{TP + TN + FP + FN} \tag{6}$$

$$\text{Precision: } PPV = \frac{TP}{TP + FP} \tag{7}$$

$$\text{Sensitivity: } TPR = \frac{TP}{P} = \frac{TP}{TP + FN} \tag{8}$$

$$\text{Fscore: } F = 2 \cdot \frac{PPV \cdot TPR}{PPV + TPR} = \frac{2TP}{2TP + FP + FN} \tag{9}$$

$$\text{MCC: } \frac{TP \cdot TN - FP \cdot FN}{\sqrt{(TP + FP)(TP + FN)(TN + FP)(TN + FN)}} \tag{10}$$

6.2 Sensitivities to methodological choices

We test the sensitivity of our results to the choice of reference interval (Supplementary Fig.S36), normalisation interval (Supplementary Fig. S35), different calibration and verification periods (Supplementary Fig. S34) and the influence of individual proxies (Supplementary Fig. S17). We find that for most of these tests there is a similar increase of CP events compared to EP El Niño events. The choice of calibration and verification period expressed by our ensemble spread (Supplementary Fig.S34) indicates a brief period in the 1680-90s of little EP activity compared with CP activity. Although the recent increase is unprecedented, some decades could potentially show similar behaviour. The 1680-90s are relatively well represented by coral records, leading to skillful reconstructions at this time. When accounting for unexplained variance as done by simulating with an AR(4) process, the number of CP El Niño events stays below 6 events per 30 years at it maximum. The effect of a varying number of coral records and therefore our nested approach is also tested based on the longest nest of records (Supplementary Fig.S34). Again, during the instrumental period the ratio of EP and CP Niño events is stable whereas in earlier decades periods of little EP activity is apparent. By varying the training period (Supplementary Fig.S33) we can see that the more training years that are used, the better the classification is in terms of detection rate. Even if we train the classification tree on only a few years prior to 1984, we see a clear increase of CP events towards the most recent decade.

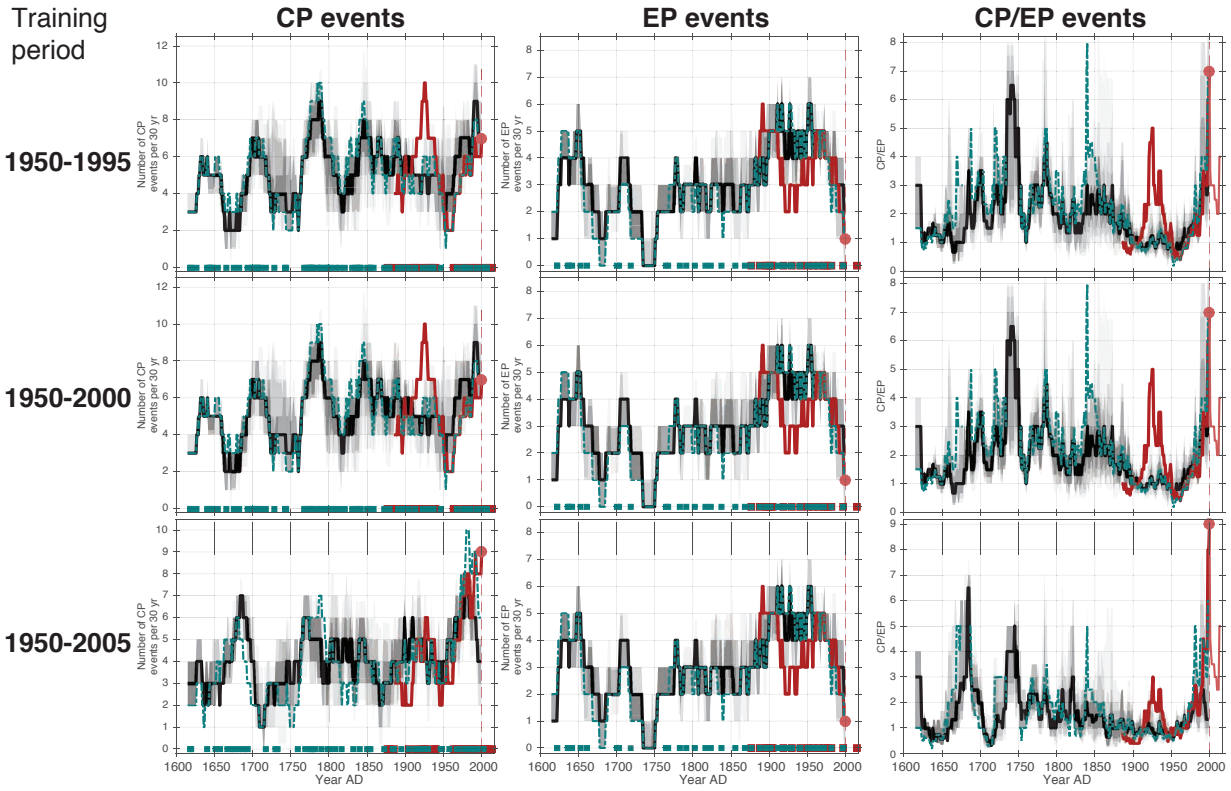

Figure S33. Sensitivity of event classification to different training periods. Number of CP El Niño events (left column), EP El Niño events (middle column) and ratio of CP to EP events (right) in sliding 30-yr windows; instrumental (red), most-replicated reconstruction (teal), bootstrapped median (black) and uncertainty range in grey shadings (75^{th}, 90^{th}, 95^{th} percentiles) shown. Different training periods (rows) are used to train the classification tree (instrumental) starting in 1950 until 1995, 2000 and 2005.

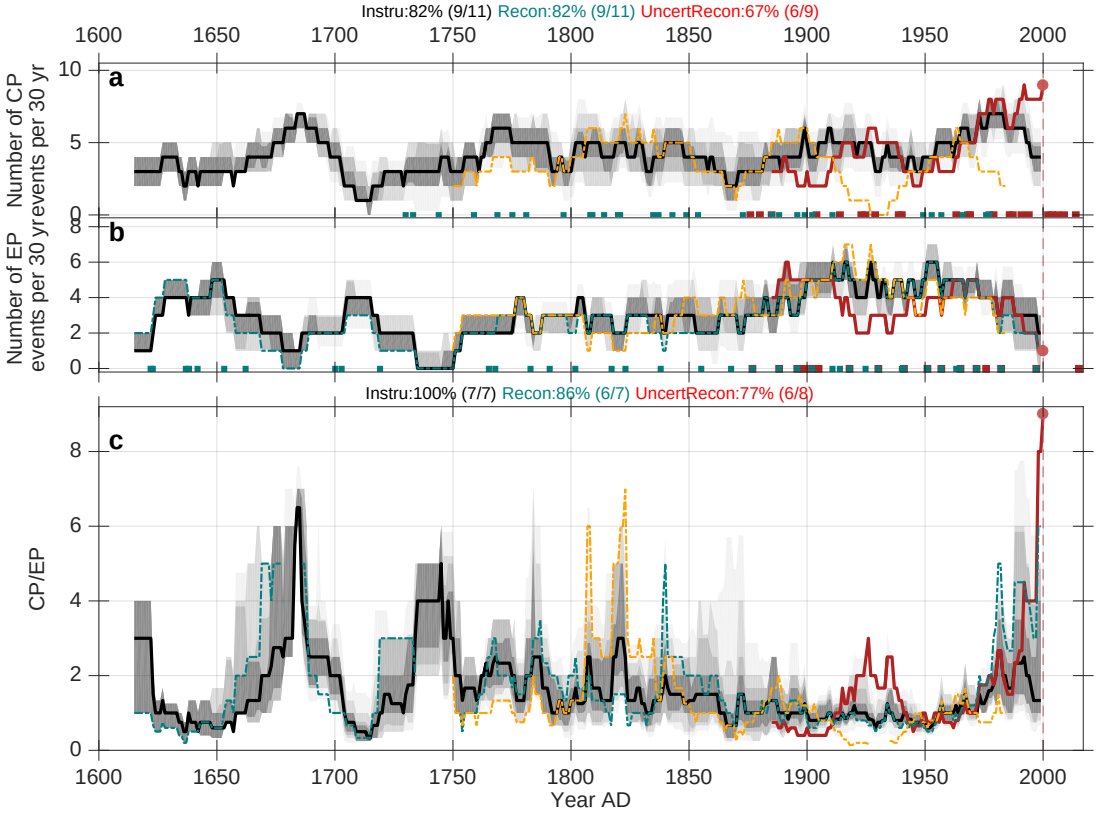

Figure S34. El Niño event diversity for a fixed nest and the ensemble range. Number of CP El Niño (**a**), EP El Niño events (**b**) and ratio of CP to EP events (**c**) in sliding 30-yr windows; instrumental (red), most-replicated reconstruction (teal), bootstrapped median (black) and uncertainty range in grey shadings (75^{th}, 90^{th}, 95^{th} percentiles) shown. Vertical red dotted line indicates most recent window, centred on 2001. El Niño events based on a long nest (fixed number of records) are shown (in yellow). The fixed nest reconstruction represents the highest time-integrated RE reconstruction based on a single set of coral records. The ensemble spread shows the uncertainty range using different calibration and verification periods. The number and percentages of correctly classified events for the instrumental record (Instru), fixed nest reconstruction (Recon) and considering uncertainties (UncertRecon) are given at the top.

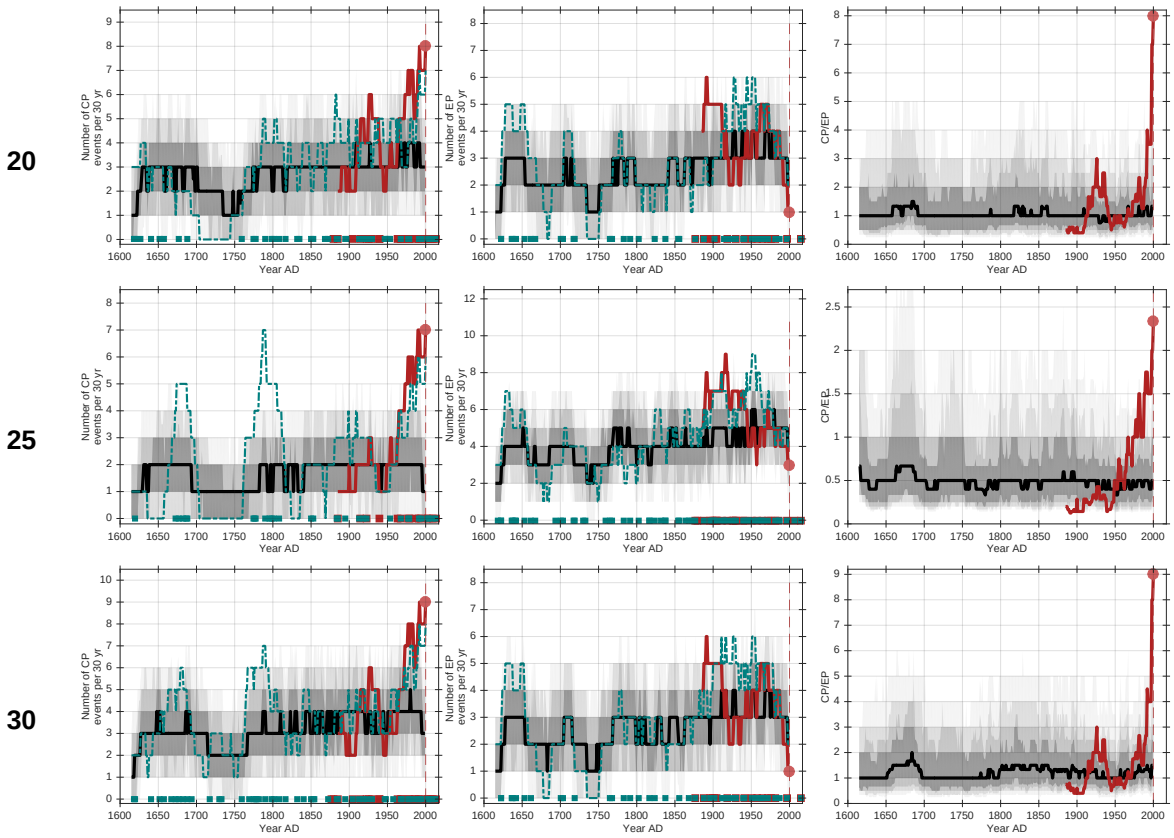

Figure S35. Sensitivity of event classification to normalisation window length. Number of CP El Niño events (left column), EP El Niño events (middle column) and ratio of CP to EP events (right) in sliding 30-yr windows; instrumental (red), most-replicated reconstruction (teal), bootstrapped median (black) and uncertainty range in grey shadings (75^{th}, 90^{th}, 95^{th} percentiles) shown. Different window length in 20, 25 and 30-year windows (rows) used for the moving normalisation of the records prior to the classification.

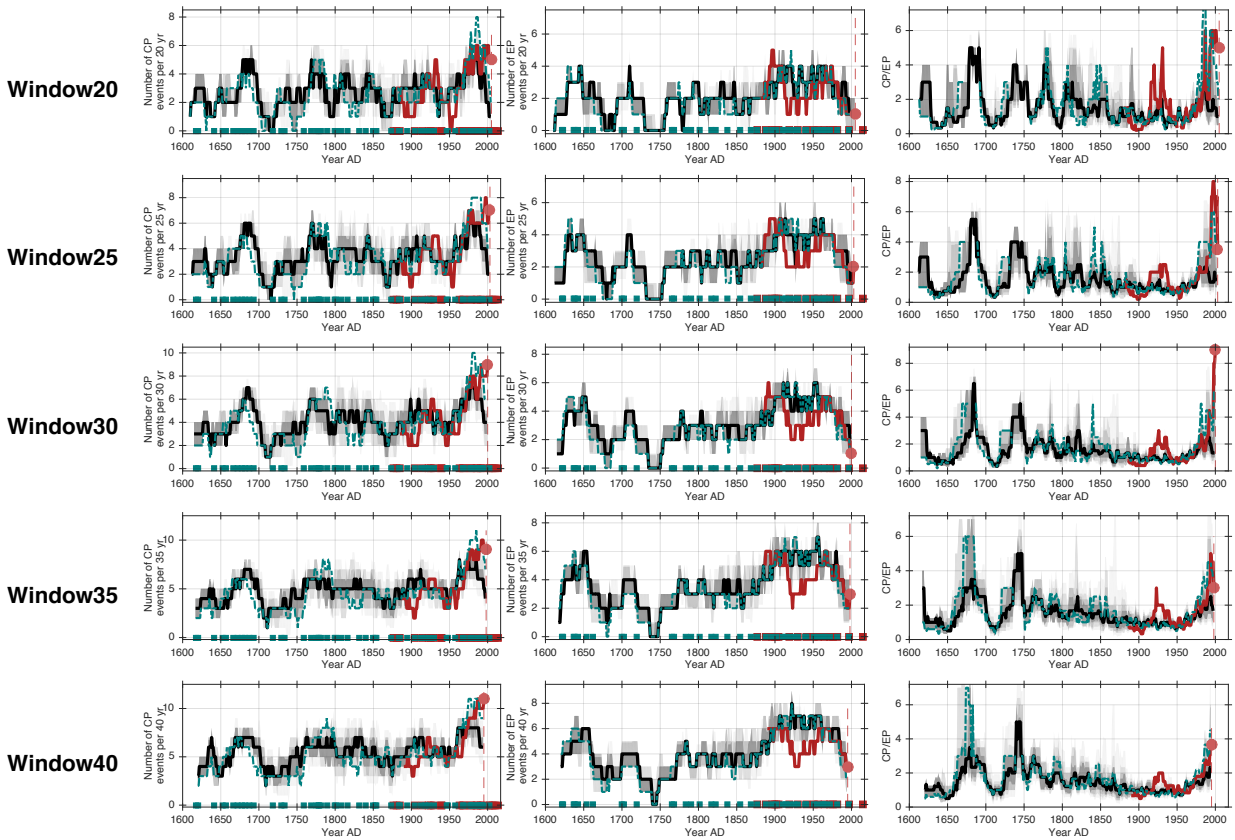

Figure S36. Sensitivity of event count to window width. Number of CP El Niño events (left column), EP El Niño events (middle column) and ratio of CP to EP events (right) in sliding 20 to 40-yr windows; instrumental (red), most-replicated reconstruction (teal), bootstrapped median (black) and uncertainty range in grey shadings (75^{th}, 90^{th}, 95^{th} percentiles) shown. Varying window width (in years) for event counts (rows).

References

[1] Kao, H.-Y. & Yu, J.-Y. Contrasting Eastern-Pacific and Central-Pacific Types of ENSO. *J. Clim.* **22**, 615–632 (2009).

[2] Yu, J.-Y. & Kim, S. T. Identification of Central-Pacific and Eastern-Pacific types of ENSO in CMIP3 models. *Geophys. Res. Lett.* **37**, L15705 (2010).

[3] Rayner, N. A., Parker, D. E. & Horton, E. B. Global analyses of sea surface temperature, sea ice, and night marine air temperature since the late nineteenth century. *J. Geophys. Res.* **108**, 4407 (2003).

[4] Trenberth, K. E. & Stepaniak, D. P. Indices of El Niño evolution. *J. Clim.* **14**, 1697–1701 (2001).

[5] Ashok, K., Behera, S. K., Rao, S. A., Weng, H. & Yamagata, T. El Niño Modoki and its possible teleconnection. *J. Geophys. Res.* **112**, C11007 (2007).

[6] Ren, H.-L. & Jin, F.-F. Niño indices for two types of ENSO. *Geophys. Res. Lett.* **38**, L04704 (2011).

[7] Kennedy, J. J. A review of uncertainty in in situ measurements and data sets of sea surface temperature. *Rev. Geophys.* **52**, 1–32 (2014).

[8] Rayner, N. A. *et al.* Improved analyses of changes and uncertainties in sea surface temperature measured in situ since the mid-nineteenth century: The HadSST2 dataset. *J. Clim.* **19**, 446–469 (2006).

[9] Osborn, T. J. & Jones, P. D. The CRUTEM4 land-surface air temperature dataset: construction, previous versions and dissemination via Google Earth. *Earth Syst. Sci. Data Discuss.* **6**, 597–619 (2014).

[10] Yasunaka, S. & Hanawa, K. Intercomparison of historical sea surface temperature datasets. *Int. J. Climatol.* **31**, 1056–1073 (2010).

[11] Huang, B. *et al.* Extended Reconstructed Sea Surface Temperature Version 4 (ERSST.v4). Part I: Upgrades and Intercomparisons. *J. Clim.* **28**, 911–930 (2015).

[12] Rasmusson, E. M. & Carpenter, T. H. Variation in tropical sea surface temperature and surface wind fields associated with the Southern Oscillation/El Niño. *Mon. Weather. Rev.* **110**, 354 (1982).

[13] Singh, A., Delcroix, T. & Cravatte, S. Contrasting the flavors of El Niño-Southern Oscillation using sea surface salinity observations. *J. Geophys. Res.* **116**, 23063–16 (2011).

[14] Gouretski, V. & Reseghetti, F. On depth and temperature biases in bathythermograph data Development of a new correction scheme based on analysis of a global ocean database. *Deep. Res. Part I* **57**, 812–833 (2010).

[15] Adler, R. F. *et al.* The version-2 global precipitation climatology project (GPCP) monthly precipitation analysis (1979-present). *J. Hydrometeorol.* **4**, 1147–1167 (2003).

[16] Yeh, S.-W., Wang, X., Wang, C. & Dewitte, B. On the Relationship between the North Pacific Climate Variability and the Central Pacific El Niño. *J. Clim.* **28**, 663–677 (2015).

[17] Wiedermann, M., Geophysical, A. R. & 2016. A climate network-based index to discriminate different types of El Niño and La Niña. *Wiley Online Libr.* **43**, 7176–7185 (2016).

[18] Banholzer, S. & Donner, S. The influence of different El Niño types on global average temperature. *Geophys. Res. Lett.* **41**, 2093–2099 (2014).

[19] Marathe, S., Ashok, K., Swapna, P. & Sabin, T. P. Revisiting El Niño Modokis. *Clim. Dyn.* 1–19 (2015).

[20] Kulkarni, M. N. & Siingh, D. The atmospheric electrical index for ENSO modoki: Is ENSO modoki one of the factors responsible for the warming trend slowdown? *Sci. Reports* **6**, 1–10 (2016).

[21] Yu, J.-Y. & Kim, S. T. Identifying the types of major El Niño events since 1870. *Int. J. Climatol.* **33**, 2105–2112 (2012).

[22] Pascolini-Campbell, M. *et al.* Toward a record of Central Pacific El Niño events since 1880. *Theor. Appl. Climatol.* **119**, 379–389 (2014).

[23] Yeh, S.-W., Wang, X., Wang, C. & Dewitte, B. On the Relationship between the North Pacific Climate Variability and the Central Pacific El Niño. *J. Clim.* **28**, 663–677 (2015).

[24] Smith, S. V., Buddemeier, R. W., Redalje, R. C. & Houck, J. E. Strontium-calcium thermometry in coral skeletons. *Sci.* **204**, 404–407 (1979).

[25] Weber, J. N. & Woodhead, P. M. Temperature Dependence of Oxygen-18 Concentration in Reef Coral Carbonates. *J. Geophys. Res.* **77**, 463–& (1972).

[26] Grottoli, A. G. & Eakin, C. M. A review of modern coral δ18O and Δ14C proxy records. *Earth-Science Rev.* **81**, 67–91 (2007).

[27] Wiedermann, M., Siegmund, J. F., Donges, J. F., Kurths, J. & Donner, R. V. Differential imprints of distinct ENSO flavors in global extreme precipitation patterns. *arXiv.org* (2017). 1702.00218v1.

[28] Cobb, K. M., Charles, C. D., Cheng, H. & Edwards, R. L. El Nino/Southern Oscillation and tropical Pacific climate during the last millennium. *Nat.* **424**, 271–276 (2003).

[29] Linsley, B. K. *et al.* Tracking the extent of the South Pacific Convergence Zone since the early 1600s. *Geochem. Geophys. Geosystems* **7**, Q05003 (2006).

[30] DeLong, K. L., Quinn, T. M., Taylor, F. W., Lin, K. & Shen, C.-C. Sea surface temperature variability in the southwest tropical Pacific since AD 1649. *Nat. Clim. Chang.* **2**, 799–804 (2012).

[31] Quinn, T. M., Crowley, T. J., Taylor, F. W. & Henin, C. A multicentury stable isotope record from a New Caledonia coral: Interannual and decadal sea surface temperature variability in the southwest Pacific since 1657 A.D. *Paleoceanogr.* **13**, 412–426 (1998).

[32] Linsley, B. K., Dunbar, R. B., Wellington, G. M. & Mucciarone, D. A. A Coral-Based Reconstruction of Intertropical Convergence Zone Variability Over Central-America Since 1707. *J. Geophys. Res.* **99**, 9977–9994 (1994).

[33] Charles, C. D., Cobb, K., Moore, M. D. & Fairbanks, R. G. Monsoon–tropical ocean interaction in a network of coral records spanning the 20th century. *Mar. Geol.* **201**, 207–222 (2003).

[34] Asami, R. *et al.* Interannual and decadal variability of the western Pacific sea surface condition for the years 1787-2000: Reconstruction based on stable isotope record from a Guam coral. *J. Geophys. Res.* **110**, C05018 (2005).

[35] Osborne, M. C., Dunbar, R. B., Mucciarone, D. A., Druffel, E. & Sanchez-Cabeza, J.-A. A 215-yr coral δ18O time series from Palau records dynamics of the West Pacific Warm Pool following the end of the Little Ice Age. *Coral Reefs* **33**, 719–731 (2014).

[36] Sanchez, S. C., Charles, C. D., Carriquiry, J. D. & Villaescusa, J. A. Two centuries of coherent decadal climate variability across the Pacific North American region. *Geophys. Res. Lett.* **43**, 9208–9216 (2016).

[37] Urban, F. E., Cole, J. E. & Overpeck, J. T. Influence of mean climate change on climate variability from a 155-year tropical Pacific coral record. *Nat.* **407**, 989–993 (2000).

[38] Gorman, M. K. *et al.* A coral-based reconstruction of sea surface salinity at Sabine Bank, Vanuatu from 1842 to 2007 CE. *Paleoceanogr.* **27**, PA3226 (2012).

[39] Linsley, B. K., Zhang, P., Kaplan, A., Howe, S. S. & Wellington, G. M. Interdecadal-decadal climate variability from multicoral oxygen isotope records in the South Pacific Convergence Zone region since 1650 A.D. *Paleoceanogr.* **23**, PA2219 (2008).

[40] Abram, N. J., Gagan, M. K., Cole, J. E., Hantoro, W. S. & Mudelsee, M. Recent intensification of tropical climate variability in the Indian Ocean. *Nat. Geosci.* **1**, 849–853 (2008).

[41] Kuhnert, H., Patzold, J., Wyrwoll, K. H. & Wefer, G. Monitoring climate variability over the past 116 years in coral oxygen isotopes from Ningaloo Reef, Western Australia. *Int. J. Earth Sci.* **88**, 725–732 (2000).

[42] Tudhope, A. W. Variability in the El Nino-Southern Oscillation Through a Glacial-Interglacial Cycle. *Sci.* **291**, 1511–1517 (2001).

[43] Nurhati, I. S., Cobb, K. M., Charles, C. D. & Dunbar, R. B. Late 20th century warming and freshening in the central tropical Pacific. *Geophys. Res. Lett.* **36**, 345–4 (2009).

[44] Wu, H. C., Moreau, M., Linsley, B. K., Schrag, D. P. & Corrège, T. Investigation of sea surface temperature changes from replicated coral Sr/Ca variations in the eastern equatorial Pacific (Clipperton Atoll) since 1874. *Palaeogeogr. Palaeoclimatol. Palaeoecol.* **412**, 208–222 (2014).

[45] Cole, J. E. & Fairbanks, R. G. The Southern Oscillation recorded in the δ18O of corals from Tarawa Atoll. *Paleoceanogr.* **5**, 669–683 (1990).

[46] Guilderson, T. P. & Schrag, D. P. Reliability of coral isotope records from the Western Pacific Warm Pool: A comparison using age-optimized records. *Paleoceanogr.* **14**, 457–464 (1999).

[47] DeLong, K. L., Quinn, T. M., Taylor, F. W., Shen, C.-C. & Lin, K. Improving coral-base paleoclimate reconstructions by replicating 350years of coral Sr/Ca variations. *Palaeogeogr. Palaeoclimatol. Palaeoecol.* **373**, 6–24 (2013).

[48] Evans, M. N., Kaplan, A. & Cane, M. A. Pacific sea surface temperature field reconstruction from coral δ 18O data using reduced space objective analysis. *Paleoceanogr.* **17**, 7–1–7–13 (2002).

[49] Evans, M. N., Kaplan, A. & Cane, M. Optimal sites for coral-based reconstruction of global sea surface temperature. *Paleoceanogr.* **13**, 502–516 (1998).

[50] Stevenson, S., McGregor, H. V., Phipps, S. J. & Fox-Kemper, B. Quantifying errors in coral-based ENSO estimates: Toward improved forward modeling of δ18O. *Paleoceanogr.* **28**, 633–649 (2013).

[51] Emile-Geay, J., Cobb, K. M., Mann, M. E. & Wittenberg, A. T. Estimating Central Equatorial Pacific SST Variability over the Past Millennium. Part II: Reconstructions and Implications. *J. Clim.* **26**, 2329–2352 (2013).

[52] Power, S., Casey, T., Folland, C., Colman, A. & Mehta, V. Inter-decadal modulation of the impact of ENSO on Australia. *Clim. Dyn.* (1999).

[53] Henley, B. J. Pacific decadal climate variability: Indices, patterns and tropical-extratropical interactions. *Glob. planetary Chang.* **155**, 42–55 (2017).

[54] Lee, T. & McPhaden, M. J. Increasing intensity of El Niño in the central-equatorial Pacific. *Geophys. Res. Lett.* **37**, L14603 (2010).

[55] Yeo, S.-R., Yeh, S.-W., Kim, K.-Y. & Kim, W. The role of low-frequency variation in the manifestation of warming trend and ENSO amplitude. *Clim. Dyn.* **49**, 1197–1213 (2016).

[56] Zhong, W., Zheng, X.-T. & Cai, W. A decadal tropical Pacific condition unfavorable to central Pacific El Niño. *Geophys. Res. Lett.* **44**, 7919–7926 (2017).

[57] Wilson, R. *et al.* Reconstructing ENSO: the influence of method, proxy data, climate forcing and teleconnections. *J. Quat. Sci.* **25**, 62–78 (2010).

[58] Ault, T. R. *et al.* Intensified decadal variability in tropical climate during the late 19th century. *Geophys. Res. Lett.* **36**, 2209–5 (2009).

[59] Giese, B. S. *et al.* The 1918/19 El Niño. *Bull. Am. Meteorol. Soc.* **91**, 177–183 (2010).

[60] Evans, M. N., Kaplan, A. & Cane, M. Intercomparison of coral oxygen isotope data and historical sea surface temperature (SST): Potential for coral-based SST field reconstructions. *Paleoceanogr.* **15**, 551–563 (2000).

[61] Beck, J. W. *et al.* Sea-Surface Temperature from Coral Skeletal Strontium/Calcium Ratios. *Sci.* **257**, 644–647 (1992).

[62] Corrège, T. Sea surface temperature and salinity reconstruction from coral geochemical tracers. *Palaeogeogr. Palaeoclimatol. Palaeoecol.* **232**, 408–428 (2006).

[63] Mathys, C. A Bayesian foundation for individual learning under uncertainty. *Front. Hum. Neurosci.* **5**, 39 (2011).

[64] Bishop, C. *Pattern Recognition and Machine Learning (Information Science and Statistics), 1st edn. 2006. corr. 2nd printing edn* (Springer, 2007).

[65] Gelman, A. *et al. Bayesian data analysis; 3rd ed.* Texts in statistical science (CRC Press, Boca Raton, FL, 2014).

[66] Drugowitsch, J. Variational Bayesian inference for linear and logistic regression. *arXiv.org* (2013). `1310.5438v2`.

[67] Daunizeau, J., Friston, K. J. & Kiebel, S. J. Variational Bayesian identification and prediction of stochastic nonlinear dynamic causal models. *Phys. D* **238**, 2089–2118 (2009).

[68] Blei, D. M., Kucukelbir, A. & McAuliffe, J. D. Variational Inference: A Review for Statisticians. *J. Am. Stat. Assoc.* **112**, 859–877 (2017).

[69] Cook, E. R., Meko, D. M., Stahle, D. W. & Cleaveland, M. K. Drought reconstructions for the continental United States*. *J. Clim.* **12**, 1145–1162 (1999).

[70] Wilks, D. S. *Statistical Methods in the Atmospheric Sciences* (Academic Press, 2011), 3 edn.

[71] Lorenz, E. N. *Empirical orthogonal functions and statistical weather prediction* (Massachusetts Institute of Technology, Department of Meteorology, 1956).

[72] Cook, E. R., Briffa, K. R. & Jones, P. D. Spatial regression methods in dendroclimatology: a review and comparison of two techniques. *Int. J. Climatol.* **14**, 379–402 (1994).

[73] Tierney, J. E. *et al.* Tropical sea surface temperatures for the past four centuries reconstructed from coral archives. *Paleoceanogr.* **30**, 226–252 (2015).

[74] Emile-Geay, J., Cobb, K. M., Mann, M. E. & Wittenberg, A. T. Estimating Central Equatorial Pacific SST Variability over the Past Millennium. Part I: Methodology and Validation. *J. Clim.* **26**, 2302–2328 (2013).

[75] Dunbar, R. B., Wellington, G. M., COLGAN, M. W. & GLYNN, P. W. Eastern Pacific Sea-Surface Temperature Since 1600-Ad - the Delta-O-18 Record of Climate Variability in Galapagos Corals. *Paleoceanogr.* **9**, 291–315 (1994).

[76] Hong-Li Ren, F.-F. J. B. T. A. A. S. Distinct persistence barriers in two types of ENSO. *Geophys. Res. Lett.* 1–7 (2016).

[77] Lever, J., Krzywinski, M. & Altman, N. Points of significance: Classification evaluation. *Nat. Methods* (2016).

[78] Stehman, S. V. Selecting and interpreting measures of thematic classification accuracy. *Remote. Sens. Environ.* **62**, 77–89 (1997).

[79] Krzywinski, M. & Altman, N. Classification and regression trees. *Nat. Methods* **14**, 755–756 (2017).